Coherent state field theory for reversible gelation of star polymers

Daniel L. Vigil,[†,¶] Glenn H. Fredrickson,[*,†,§] and Jian Qin[*,‡]

†*Department of Chemical Engineering, University of California, Santa Barbara, CA 93106, USA*

‡*Department of Chemical Engineering, Stanford University, Stanford, CA 94305, USA*

¶*KBR Inc., Intelligent Systems Division, NASA Ames Research Center, Mountain View, CA 94035, USA*

§*Department of Chemical Engineering and Materials Research Laboratory, University of California, Santa Barbara, CA 93106, USA*

E-mail: ghf@ucsb.edu; jianq@stanford.edu

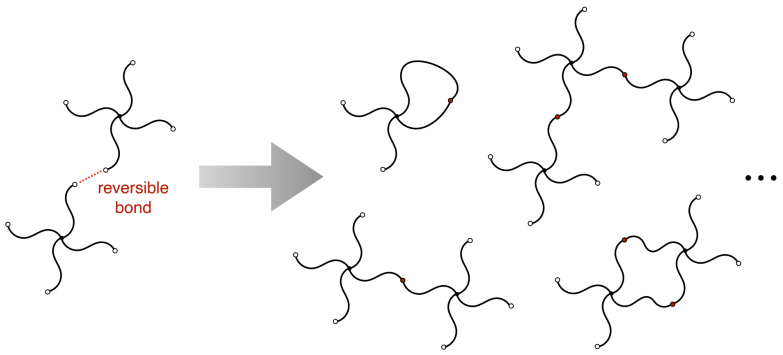

(TOC graphic)

Abstract

A coherent states field theory (CST) framework for reversible gelation of end-functional f-arm stars is presented, which implicitly enumerates all cross-linking patterns and generates the correct statistical weight for each type of cluster. At the mean-field level, the CST produces only tree-like clusters, and recovers all essential predictions of the Flory-Stockmayer (FS) theory. In particular, the saddle-point (mean-field) condition reproduces the FS condition for gelation. When applied to solutions of associative polymer stars in an implicit solvent, this mean-field theory predicts a two-phase region where sol and gel phases of different composition coexist. Beyond the mean-field level, where both tree and loop-like clusters are present, we develop a loop density operator by considering the spatial translation of finite clusters. The field theory is then fully developed and analyzed at the Gaussian level of fluctuations. Phantom stars, dilute solutions, and dense melts are studied to better understand the predictions of the Gaussian theory, including those for the loop density and fluctuation corrections to the cluster number density. It is shown that the contributions from the excluded volume interaction do not affect the density of loops at the Gaussian level, although they do affect the bonding probability.

1. Introduction

Polymer networks are a fundamental platform for many important modern materials, including rubber tires, artificial tissues, structural and dental composites, and adsorbents. In recent years, polymer networks that are formed from reversible bonds have become a topic of interest. This is in part due to novel materials properties, such as self-healing[1] and stimuli-responsive behaviors, as well as biologically-motivated observations of such phenomena.[2] Much of our understanding of polymer networks is due to theories by Flory[3] and Stockmayer,[4] who performed pioneering work based on combinatorial counting of molecular clusters, which were later simplified by using iterative arguments.[5,6] They were able to show

that at a particular extent of reaction, the average size of a polymer cluster diverges, indicating the onset of gelation and the formation of a macroscopic sized molecule. Notably, there are a number of deficiencies with Flory-Stockmayer (FS) theory, mainly that it neglects the formation of cyclic (loop and ring) structures, and does not account for excluded volume or other interactions between polymer segments. Finally, it is fundamentally a mean-field theory for homogeneous systems that neglects the role of fluctuations or spatial gradients of density or composition. These can be important both in solvated and dry networks.

There have been a number of efforts to correct the FS theory for excluded volume, fluctuations, or inhomogeneities in both permanent and reversible networks, which often invoke field-based methods. One example is work by Lubensky and Isaacson who used an n-vector model and applied the $n \to 0$ formalism of de Gennes[7,8] to the problem of reversible gelation. They utilized analytical approximations to study dilute gels and compute correlation lengths, but did not analyze phase separation behavior or the concentrated regime. Because of reliance on a zero-component field theory, the approach does not enable numerical representation or investigation.

Other examples include work by Panyukov and Rabin that used replica field theory to predict structure factors and elastic properties of permanent gels with quenched disorder.[9] Goldbart and Goldenfeld focused on the qualitative feature of how rigidity emerges at the transition point, due to both crosslinking and entanglement.[10,11] They adapted the replica trick for spin glass to randomly crosslinked polymers, and constructed a mean-field theory that yields the same gel point as the FS theory. These works were also limited to approximate analytical techniques, however, and did not analyze phase separation behavior. A related study by Erukhimovich considered the possibility of loop formation, but is based on an approximate Hamiltonian that splits the contributions from short-ranged interaction and polymer connectivity, and that relies on the explicit enumeration of crosslinking topology.[12,13] Lang and co-authors have conducted a series of studies using both mean-field population balance models and spatially-resolved bond-fluctuation model Monte Carlo simulations to

interrogate the effect of loop formation on network properties, however these studies have also neglected the effects of phase behavior.[14–18]

Mohan, Mester, and Fredrickson[19,20] extended the FS theory to treat inhomogeneous reversible gels and networks, preserving the tree approximation (no cyclic reaction products), but allowing for arbitrary density or composition gradients. Within the mean-field approximation, this framework enabled a detailed study of phase behavior, including rich multicritical phenomena with competing tendencies for microphase and macrophase separation behavior in heterogeneous networks. However, numerical work with this approach is inefficient due to the need to solve nonlinear integral equations at each field update. Furthermore, the method cannot be easily extended beyond the tree approximation.

The "coherent states" (CS) framework enables a field-theoretic representation of reversible gels and networks with more favorable characteristics, namely that it exactly enumerates all clusters irrespective of topology, can address inhomogeneities, and enables efficient numerical investigation. This framework was originally introduced by Edwards and Freed for studying vulcanization.[21] The coherent states name derives from path integral descriptions of quantum many-body systems with a similar mathematical structure.[22] The CS representation of classical polymers has largely gone unnoticed for many years, especially compared to auxiliary field theory representations popularized by Edwards.[23] As described in recent publications from the Fredrickson group,[24–28] the CS framework is especially well suited for tackling systems of reversibly bonding polymers that exhibit complex self-assembly and phase behavior coupled to the reaction equilibria.

In this work we apply the CS formalism to study reversible polymer networks in solution and melt conditions and examine both gelation and phase separation. These two phenomena often occur simultaneously in polymer[29,30] and colloid solutions[31,32] and are often associated with long relaxation times and hysteresis, leading to confusion on their relationship. With the models considered here we are able to interrogate the equilibrium behavior without kinetic limitations, and also examine effects of excluded volume, rings, and fluctuations.

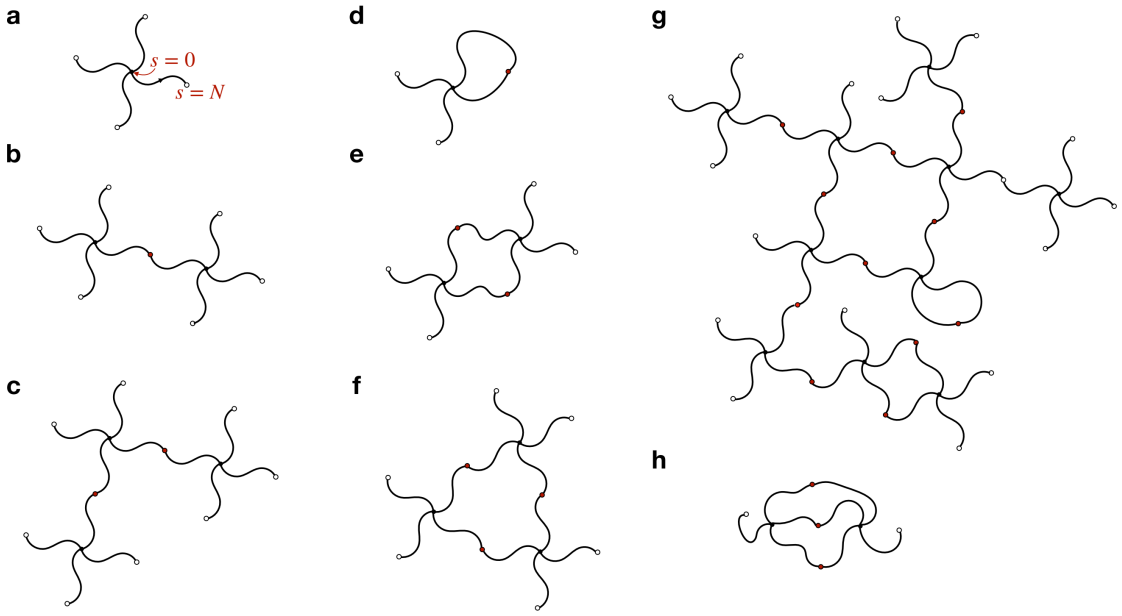

Figure 1: Examples of clusters formed by association of star polymers. (a) An example of f-arm star with $f = 4$. Arm contour is parametrized by s, with $0 \leq s \leq N$. (b) Dimer tree-like cluster. (c) Trimer tree-like cluster. (d) An intra-star loop by self-association. (e) An inter-star loop formed by linking two stars. (f) A loop formed from three stars. (g) A cluster formed from 10 stars that contains one intra-star loop, one inter-star loop formed from two stars, and one inter-star loop formed from four stars. (h) Two loops formed between two stars sharing fractions of borders or edges.

We start at the mean-field level and show that a reduced set of parameters can be defined from the fundamental parameters of reaction equilibrium constant, polymer concentration, and solvent quality to yield a universal phase diagram. We then examine the fluctuation corrections. First, an operator counting loop number density is introduced by considering cluster translational degrees of freedom. Next, the Gaussian level fluctuation about the mean-field solution is worked out, and is applied to analyze the behavior of phantom stars, dilute stars, and stars in dense melts. The contributions from loops and bonds are considered separately.

2. Model

We consider solutions of f-arm stars with equal length arms and functional groups at the terminus of each arm capable of pairwise, reversible binding. The solvent is treated implicitly and the arms are modeled as continuous Gaussian chains. The contour variable s along the arms initiates at the star center at $s = 0$ and terminates at the arm end at $s = N$ (Fig. 1a). The field theory model can be formulated in either the canonical (CE) or grand canonical ensemble (GCE). The GCE proves slightly more convenient for our purposes, so is used as the starting point, but the transition to the CE involves changing only one term in the Hamiltonian functional, and will be described when necessary in the following.

The field-theoretic representation that we employ is not a pure CS representation, but is an example of a "hybrid" auxiliary field-coherent states field theory (AF-CS) where a real auxiliary field $w(\mathbf{r})$ is used to decouple the pairwise excluded volume interactions and two complex-conjugate CS fields $\phi^*(\mathbf{r}, s)$ and $\phi(\mathbf{r}, s)$ are used to build the star polymers and all possible clustered reaction products. Such hybrid representations have been derived and discussed for both continuous and discrete chain models in the recent monograph by Fredrickson and Delaney.[27] The GCE partition function Ξ for the star polymer model of interest has the form

$$\Xi(\lambda_\mathrm{b}, \lambda_f, V) = \int \frac{\mathcal{D}[w]}{D_w} \int \frac{\mathcal{D}[\phi, \phi^*]}{D_\phi} \exp\left(-H[\phi, \phi^*, w]\right) \tag{1}$$

$$\begin{aligned} H[\phi, \phi^*, w] = \frac{1}{2u_0} \int \mathrm{d}\mathbf{r}\, w(\mathbf{r})^2 + \int \mathrm{d}\mathbf{r} \int \mathrm{d}s\, \phi^*(\mathbf{r}, s) \left[\mathcal{L} + \mathrm{i}w(\mathbf{r})\right] \phi(\mathbf{r}, s) \\ - \int \mathrm{d}\mathbf{r} \left(\frac{\lambda_f}{f!} \phi^*(\mathbf{r}, 0)^f + \phi(\mathbf{r}, N) + \frac{\lambda_\mathrm{b}}{2!} \phi(\mathbf{r}, N)^2 \right) \end{aligned} \tag{2}$$

where $\int \mathcal{D}[w]$ and $\int \mathcal{D}[\phi, \phi^*]$ denote functional integrals over the AF and CS fields, respectively, and H is the effective Hamiltonian functional. Here, λ_b and λ_f are activities of reversible bonds and stars, and V is the system volume. Throughout this work, we set $k_\mathrm{B}T = 1$ and suppress the reference to temperature T. The domain of integration for the

spatial coordinate $\mathbf{r}$ is the system volume, and that of the contour variable s is from $s = 0$ to N.

The effective Hamiltonian in eq. (2) has three contributions. The first term depending on w^2 represents the segmental interactions, which has the pseudo-potential form $u_0\delta(\mathbf{r})$ for two segments separated by displacement $\mathbf{r}$, where $\delta(\mathbf{r})$ is the Dirac delta function. The excluded volume strength u_0 (here assumed positive) depends on the solvent quality and can be inferred from the potential of mean force between a pair of star polymer segments. Introducing the auxiliary field w allows for decoupling the non-bonded interactions among segments, at the cost of introducing the new functional integral over $w(\mathbf{r})$.

The second term in H represents an "ideal arm" modeled as a continuous Gaussian chain with each segment experiencing a pure imaginary effective potential $\mathrm{i}w(\mathbf{r})$. The operator $\mathcal{L} = \frac{\partial}{\partial s} - \frac{b^2}{6}\nabla^2$ propagates chain conformation, where b is the statistical segmental length. The operator $\mathcal{L}$ is the only place where molecular conformation statistics enter the theory and provides the only nonlocal contribution. Proper treatment of the non-Hermitian operator $\frac{\partial}{\partial s}$ ensures that, when second moments of the coherent fields are evaluated, only pair correlation terms of the form $\langle\phi(\mathbf{r}, s)\phi^*(\mathbf{r}', s')\rangle$ with $s > s'$ survive due to causality. All other pairwise averages that violate this condition or involve the products $\phi\phi$ or $\phi^*\phi^*$ vanish. The coupling with field $\mathrm{i}w$ can also be written in terms of the segmental density operator $\rho(\mathbf{r}) \equiv \int \mathrm{d}s\, \phi^*(\mathbf{r}, s)\phi(\mathbf{r}, s)$ as $\int \mathrm{d}\mathbf{r}\, \mathrm{i}w(\mathbf{r})\rho(\mathbf{r})$. In the absence of the term $\mathrm{i}w$, the second term of eq. (2) represents the contributions of non-interacting or "phantom" arms. It is worth noting that the w integral in the partition function is Gaussian and could be explicitly performed, simplifying the hybrid AF-CS field theory to a "pure" CS form. However, we resist this step as it serves to facilitate the Gaussian fluctuation analysis of Section V.

The third "source" term of H defines the structure and the association reactions for the stars. The activity-dependent term $\frac{\lambda_f}{f!}\phi^*(\mathbf{r}, 0)^f$ generates the cores (centers) of the f-arm stars. The normalizing factor of $\frac{1}{f!}$ accounts for the indistinguishability of the f identical arms emanating from each star center. Each arm is terminated either as a free end, via the

term $\phi(\mathbf{r}, N)$, or is bonded to another arm end via $\frac{\lambda_\mathrm{b}}{2!}\phi(\mathbf{r}, N)^2$. The number of reversible bonds is controlled by the bond activity λ_b. These bonds can be either intra-molecular or inter-molecular allowing the creation of both networks and isolated polymer molecules or clusters with cyclic structures (loops). By means of a perturbation expansion in the source term, it can be shown that this model correctly generates all possible reaction products with proper classical statistical mechanical weighting. The products generated follow an "equal reactivity" scheme whereby the equilibrium constant for each possible association reaction is identical and proportional to λ_b.

To obtain the partition function of the CE, we Taylor-expand the GCE partition function in powers of activity $\frac{\lambda_f}{f!}$. The n-th order coefficient is the CE partition function for n stars contained in the volume V. The net result amounts to replacing only the λ_f-dependent term in the GCE Hamiltonian with

$$-n \ln \left(\frac{1}{V} \int \mathrm{d}\mathbf{r}\, \phi^*(\mathbf{r}, 0)^f \right) \tag{3}$$

where the factor of $1/V$ has been inserted to extract the ideal gas contribution of n non-interacting star polymers from the CE partition function. Strictly speaking, this CE representation is a semi-grand canonical ensemble where the total number of stars is fixed at n, but the relative activity of each possible product is specified to ensure reaction equilibrium. A true canonical ensemble would specify the number of each possible product and have a quenched product distribution.

Finally, the normalizing factors in the partition function ensure the existence of the partition function in the continuum limit of functional integrals and are defined as follows

$$D_w \equiv \int \mathcal{D}[w] \exp \left(-\frac{1}{2u_0} \int \mathrm{d}\mathbf{r}\, w(\mathbf{r})^2 \right) \tag{4}$$

$$D_\phi \equiv \int \mathcal{D}[\phi, \phi^*] \exp \left(-\int \mathrm{d}\mathbf{r} \int \mathrm{d}s\, \phi^*(\mathbf{r}, s)\, \mathcal{L}\, \phi(\mathbf{r}, s) \right) \tag{5}$$

It can be verified that the expression for the Hamiltonian is compatible with the following unit convention that we adopt for physical properties: $[w] = [\phi^*] = 1$, $[u_0] = [\lambda_\mathrm{b}] =$ volume, and $[\phi] = [\lambda_f] = \frac{1}{\text{volume}}$, which ensures that the density $\rho \sim \phi^*\phi$ has the dimension of inverse volume.

Finally, we note that this model is exactly equivalent to a traditional auxiliary field (AF) model that can be expressed as

$$\Xi(\lambda_\mathrm{b}, \lambda_f, V) = \frac{1}{D_w} \int \mathcal{D}[w] \, \exp\left(-H_\mathrm{AF}[w]\right) \tag{6}$$

$$H_\mathrm{AF}[w] = \frac{1}{2u_0} \int \mathrm{d}\mathbf{r} \, w(\mathbf{r})^2 - \sum_j z_j V Q_j[\mathrm{i}w] \tag{7}$$

where the second term in eq. (7) represents a sum over all possible reaction products in the system. Each product is associated with an activity z_j and single chain partition function Q_j. For the reactive stars considered here with $f \geq 2$, this is an infinite sum, which limits the utility of the AF model. Nevertheless, it can be shown analytically that the path integral over $[\phi, \phi^*]$ in eq. (1) generates the infinite sum in eq. (7).

2.1 Equations of state

The partition function in the GCE is directly related to the osmotic pressure Π, via

$$\Pi = \frac{1}{V} \ln \Xi \tag{8}$$

When all non-bonded interactions and reactions are turned off, no w dependent terms are needed and the bond activity λ_b becomes zero. The GCE partition function can then be calculated analytically, giving $\Xi = \exp\left(\frac{\lambda_f}{f!} V\right)$ and $\Pi = \frac{\lambda_f}{f!} = \frac{n}{V}$, with n the average number of polymers, i.e., the ideal gas law. In the general case, the model is specified by two

equations of state, derived from the dependence on λ_f and λ_b respectively:

$$\rho_f = \frac{\lambda_f}{f!\,V}\int \mathrm{d}\mathbf{r}\,\langle \phi^*(\mathbf{r},0)^f\rangle = \lambda_f \frac{\partial \Pi}{\partial \lambda_f} \tag{9}$$

$$\rho_\mathrm{b} = \frac{\lambda_\mathrm{b}}{2!\,V}\int \mathrm{d}\mathbf{r}\,\langle \phi(\mathbf{r},N)^2\rangle = \lambda_\mathrm{b} \frac{\partial \Pi}{\partial \lambda_\mathrm{b}} \tag{10}$$

Here and hereafter, the thermal averages are defined as usual, and evaluated over the field variable integrals weighted by the Boltzmann factor. Equation (9) gives the volume average for the number density of stars ρ_f and, effectively, that for the segmental number density ρ by the stoichiometric relation $\rho = fN\rho_f$. Equation (10) gives the corresponding density for the number of bonds ρ_b. From these two densitites, the number density of free ends is deduced as $\rho_\mathrm{e} = f\rho_f - 2\rho_\mathrm{b}$, which can also be obtained from a field average

$$\rho_\mathrm{e} = \frac{1}{V}\int \mathrm{d}\mathbf{r}\,\langle \phi(\mathbf{r},N)\rangle \tag{11}$$

The conversion of end groups used in the literature, or bonding probability, can be defined as

$$p \equiv \frac{2\rho_\mathrm{b}}{f\rho_f} = \frac{2\rho_\mathrm{b}}{\rho/N} \tag{12}$$

In an inhomogeneous system, the local segmental densities can be expressed using the CST field average as $\rho(\mathbf{r}) = \int \mathrm{d}s\,\langle \phi^*(\mathbf{r},s)\phi(\mathbf{r},s)\rangle$. The volume average of this segment density will generate an identical result as deduced from ρ_f. We will demonstrate this explicitly in the section on the mean-field solution, and merely note that ρ_f and ρ_b are the two fundamental state variables. In practice, we found it convenient to parametrize the state using the segmental density ρ and the reaction conversion p, which should become clear in the results section.

In the CE formulation with partition function $Z(\lambda_b, n, V)$,[25,27] the equation of state for bond number density has the same form as eq. (10). Differentiating the Helmholtz free energy $F = -\ln Z$ with respect to the number of stars n, gives the following form of the

chemical potential

$$\mu = \frac{\partial F}{\partial n} = \ln(\rho_f v) - \left\langle \ln\left(\frac{1}{V}\int \mathrm{d}\mathbf{r}\, \phi^*(\mathbf{r},0)^f\right)\right\rangle \tag{13}$$

The first term is the ideal gas contribution, in which v is a normalization factor analogous to the cube of the thermal de Broglie wavelength and does not affect the thermodynamic properties. The second term is an excess contribution representing the contributions of reaction and non-bonded interactions. At the mean-field level, where the field $\phi^*(\mathbf{r},0)$ is replaced by a stationary (non-fluctuating) value at the saddle point, the argument of the logarithmic term in eq. (13) can be related to ρ_f by eq. (9). The explicit dependence on ρ_f in the ideal gas and excess contributions cancel out, giving rise to $\mu = \ln\left(\frac{\lambda_f}{f!}v\right)$. This relation and eq. (9) will facilitate the conversion of thermodynamic potentials between the GCE and CE ensembles.

3. Mean field theory

The mean-field theory of the CS model is worked out in this section, which reveals transparently the connection with the FS theory and forms the basis for the fluctuation theory developed in the following sections. Following the standard approach,[27] we seek a solution to the saddle point conditions for all the field variables

$$\begin{aligned}
\left.\frac{\delta H}{\delta \phi^*(\mathbf{r},s)}\right|_{\phi_0,\phi_0^*,w_0} &= 0 \\
\left.\frac{\delta H}{\delta \phi(\mathbf{r},s)}\right|_{\phi_0,\phi_0^*,w_0} &= 0 \\
\left.\frac{\delta H}{\delta w(\mathbf{r})}\right|_{\phi_0,\phi_0^*,w_0} &= 0
\end{aligned} \tag{14}$$

Throughout this work, we focus on a spatially homogeneous solution represented by $\phi_0(s)$, $\phi_0^*(s)$, and w_0, and use a subscript "0" to indicate properties evaluated at the mean-field

level, in particular the segmental density ρ_0 and the bonding probability p_0. Without spatial variation, the conditions eq. (14) simplify to first order ODEs for the CST fields and an algebraic condition for w_0:[25]

$$\begin{aligned}
\partial_s \phi_0(s) &= -w_0\, \phi_0(s) + \frac{\lambda_f}{(f-1)!} \phi_0^*(0)^{f-1} \delta(s) \\
\partial_s \phi_0^*(s) &= \quad w_0\, \phi_0^*(s) - [1 + \lambda_\mathrm{b} \phi_0(N)]\, \delta(N-s) \qquad (15) \\
w_0 &= u_0 \rho_0 \qquad (16)
\end{aligned}$$

The segmental density ρ_0 in the last line is calculated from $\rho_0 = \int \mathrm{d}s\, \phi_0 \phi_0^*$. The source terms in the pair of conditions for the CST fields are derived from the causality requirements: $\phi(s) = 0$ for $s < 0$ since no arm can be terminated before initiated, and $\phi^*(s) = 0$ for $s > N$ since no arm initiation is permitted after termination.

The solutions to eqs. (15) is readily found, and can be expressed in terms of segmental density ρ_0 and bonding probability p_0 as follows

$$\begin{aligned}
\phi_0(s) &= \frac{p_0\, \mathrm{e}^{-u_0 \rho_0 s}}{\tau \lambda_\mathrm{b} (1-p_0)}\, \Theta(s) \\
\phi_0^*(s) &= \frac{\tau \mathrm{e}^{u_0 \rho_0 s}}{1-p_0}\, \Theta(N-s) \qquad (17)
\end{aligned}$$

where $\Theta(s)$ is the unit step function. The step functions restrict the chain contour variable to the physical interval $0 \le s \le N$ and provide no contributions to physical quantities outside this range. The auxiliary parameter τ is the Boltzmann weight for the excluded volume interaction, $\tau \equiv \mathrm{e}^{-u_0 \rho_0 N}$. The bonding probability p_0 relates to the mean-field solution via eq 12

$$p_0 = \frac{\tau^2 \lambda_\mathrm{b} \lambda_f}{(f-1)!} \phi_0^*(0)^{f-2} \qquad (18)$$

It is clear from eqs. (17) that the product $\phi_0(s)\phi_0^*(s)$ is independent of s, as expected for a

homogeneous solution. Thus, the segmental density $\rho_0 = \int \mathrm{d}s\, \phi_0(s)\phi^*(s)$ evaluates to

$$\frac{\rho_0}{N} = \frac{p_0}{\lambda_\mathrm{b}(1-p_0)^2} \tag{19}$$

Equivalently, the density can be written using eq. (9) as $\frac{\rho_0}{N} = \frac{\lambda_f}{(f-1)!}\phi_0^*(0)^f$. It can be verified that this expression and eq. (19) are compatible by substitution of eq. (18) and $\phi_0^*(0) = \frac{\tau}{1-p_0}$, the latter derived from eq. (17).

To understand why the expression eq. (18) can be assigned to the bonding probability, we notice that eq. (10) for bond density evaluates to $\frac{\lambda_\mathrm{b}}{2}\phi_0(N)^2 = \frac{p_0^2}{\lambda_\mathrm{b}(1-p_0)^2}$ at the mean-field level. Taking the ratio of bond density and $\frac{\rho_0}{N}$ by following eq. (12) yields precisely p_0. Therefore, eq. (18) gives the mean-field expression for the probability of an end group being bonded. Noticing further that $\frac{\rho_0}{N}$ is the density of end groups, the equation of state eq. (19) can be interpreted as the law of mass action (LMA): the products $p_0\frac{\rho_0}{N}$ and $(1-p_0)\frac{\rho_0}{N}$ are the concentrations of reacted and open groups, respectively.

Equations (18) and (19) play the same role as the equations of states, eqs. (9) and (10), but are more convenient to use. In practice, we obtain p_0 by keeping the physical solution to the quadratic eq. (19) for the prescribed value of density ρ_0 and reactivity λ_b, then substitute p_0 into eq. (17) to get a unique solution for the CST fields at the saddle point.

3.1 Thermodynamics of star-polymer solution

Using the mean-field solution eq. (17), it is straightforward to evaluate eq. (2) to obtain the value of the Hamiltonian at the saddle point, which then leads to the mean-field expression for the osmotic pressure,

$$\Pi_0 = \frac{1}{V}\ln \Xi_0 = \frac{\rho_0}{N_\mathrm{n}} + \frac{u_0}{2}\rho_0^2 \tag{20}$$

Here $N_\mathrm{n} = \frac{fN}{1-p_0 f/2}$ is the number average molecular weight of the clusters formed due to end-association, i.e., the Carothers equation.[33] The ratio $\frac{\rho_0}{N_\mathrm{n}}$ is the number density of crosslinked

clusters, so the first term in eq. (20) is an ideal gas contribution. The second term is the correction due to binary segmental interactions. Equation (20) reduces to the osmotic pressure of non-associating stars[25] by setting $p_0 = 0$. At the mean-field level, the difference between non-associating and associative systems is solely contained in the term N_n. Notice that N_n apparently diverges at $p_0 = 2/f$, which is an artifact of the mean-field statistics. Strictly speaking, this expression for N_n holds only below the gel point, while the predicted divergence in N_n occurs above the gel point.

To obtain the density-explicit equation of state, we begin with the expression for chemical potential derived from eq. (13) and the discussion therein, $\mu = \ln\left(\frac{\lambda_f}{f!}v\right)$. The activity λ_f can be expressed in terms of density via eq. (9), in which $\phi_0^*(0)$ is given by eq. (17) as $\phi_0^*(0) = \frac{\tau}{1-p_0}$. By substitution, we obtain $\frac{\lambda_f}{f!} = \rho_f \left(\frac{1-p_0}{\tau}\right)^f$ and subsequently

$$\mu = \ln\left[v\rho_f(1-p_0)^f\right] + u_0\rho_0 N f \tag{21}$$

Since $\rho_f(1-p_0)^f$ is the density of un-associated stars, the above expression can be understood as the sum of ideal gas and interaction contributions to chemical potential.

By invoking a Legendre transform to the GCE potential, we obtain the following expression for the Helmholtz free energy at the mean-field level,

$$\begin{aligned}\frac{F_0}{V} &= \mu\rho_f - \Pi_0 \\ &= \rho_f \ln\left[v\rho_f(1-p_0)^f\right] - \frac{\rho_0}{N_\mathrm{n}} + \frac{u_0}{2}\rho_0^2\end{aligned} \tag{22}$$

The density of stars is related to segmental density through $\rho_f = \frac{\rho_0}{fN}$. In the limit of non-associating stars, eq. (22) reduces to a familiar mean-field expression $\rho_f \ln(v\rho_f/\mathrm{e}) + \frac{u_0}{2}\rho_0^2$, the sum of an ideal gas contribution and a binary interaction term. Equation (22) agrees with the mean-field free energy derived for a solution of associative linear polymers[29] when the densities of reacting groups, $\frac{c}{l}$ for linear chains[29] and $\frac{\rho_0}{N}$ for our star polymers, are set equal.

It is worth noting that the Helmholtz free energy is fully specified by the density ρ_0, while

the probability p_0 is constrained by the LMA. Equation (19) implies that,

$$\frac{\partial p_0}{\partial \rho_0} = \frac{p_0(1-p_0)}{\rho_0(1+p_0)} \tag{23}$$

which can be used to handle the implicit dependence of p_0 on ρ_0 while λ_b is fixed. For instance, it allows us to verify that eq. (21) can also be derived from $\mu = \frac{\partial F_0}{\partial n} = \frac{\partial (F_0/V)}{\partial \rho_f}$. More importantly, by differentiation, we obtain the following expression for the inverse of the osmotic compressibility,

$$\frac{\mathrm{d}\mu}{\mathrm{d}\rho_0} = \frac{1}{\rho_0 N_w} + u_0 N f \tag{24}$$

in which $N_w = fN\frac{1+p_0}{1-(f-1)p_0}$ is the weight-average molecular weight of associated stars predicted by the FS theory.[34] In fact, the Helmholtz free energy is the generating function for the moments of associated clusters. The next order of differentiation with respect to ρ_0 gives the z-average molecular weight, depending on N_z/N_w^2, etc.

The weight average N_w diverges at $p_0 = (f-1)^{-1}$, the gel point predicted by the FS theory.[3,35,36] It shows the consistency between our thermodynamic theory and the FS argument based on percolation structure. For non-vanishing u_0, setting the inverse osmotic compressibility to vanish gives the following expression for the stability limit of a homogeneous mixture, i.e., the spinodal condition,

$$1 - (f-1)p_0 + u_0(Nf)^2\rho_f(1+p_0) = 0 \tag{25}$$

The dependence on u_0 (> 0) shows the contribution from the excluded volume interaction; consequently the value of p_0 at the spinodal is always above the gel point $(f-1)^{-1}$. The competition between gelation and phase separation will be discussed below.

3.2 Order parameter for gelation

We show in this section how the fraction of the star polymers that reside in the *gel* or *sol*, $P_{\rm gel}$ or $P_{\rm sol}$, emerges from the saddle point condition for the CST fields. Polymers belonging to infinite (percolating) clusters constitute the gel fraction, while the sol fraction is comprised of isolated stars and clusters of finite molecular weight. The two fractions are complementary, so we can focus on, e.g., $P_{\rm sol}$ alone and denote it the order parameter of gelation. Below the gel point $p_0 = \frac{1}{f-1}$, $P_{\rm sol} = 1$; above the gel point, $P_{\rm sol}$ decreases monotonically with p_0 and reaches zero at $p_0 = 1$ according to the FS theory. This trend is exhibited in Fig. 2 for $f = 3$ and 5.

Next, we show how this characteristic P_{sol} behavior is obtained from the mean-field CST equations, eqs. (17–19). For any prescribed segmental density $\frac{\rho_0}{N}$ and bond fugacity $\lambda_{\rm b}$, a solution for p_0 can be found from the LMA, eq. (19). The conversion p_0 can then be substituted to eq. (17) to find the CST fields, and to eq. (18) to further find λ_f. The solution is unique: for given $\frac{\rho_0}{N}$ and $\lambda_{\rm b}$, only one set of p_0, $\phi_0(s)$, $\phi_0^*(s)$, and λ_f can be found.

To reveal the piecewise expression for $P_{\rm sol}$ spanning the gel point, we examine the saddle point condition more closely. Equations (17) and (18) can be combined to yield the condition for $\phi_0^*(0)$,

$$\frac{\phi_0^*(0)}{\tau} - 1 = \frac{\lambda_{\rm b}\lambda_f \tau^f}{(f-1)!}\left(\frac{\phi_0^*(0)}{\tau}\right)^{f-1} \tag{26}$$

Substitution of $\phi_0^*(0) = \frac{\tau}{1-p_0}$ into eq. (18) leads to $\frac{\lambda_{\rm b}\lambda_f\tau^f}{(f-1)!} = p_0(1-p_0)^{f-2}$. Then noticing that $\tau = {\rm e}^{-u_0\rho_0 N}$ is a constant, we denote $x \equiv \phi_0^*(0)/\tau$ for convenience and write eq. (26) as $x - 1 = c\,x^{f-1}$, where $c \equiv p_0(1-p_0)^{f-2}$. This equation has a unique solution for x in the cases of $f = 1$ and 2. For $f \geq 3$, we show in section S1.1 that eq. (26) has two, one, and zero positive roots for $c < c_{\rm g}$, $c = c_{\rm g}$, and $c > c_{\rm g}$ respectively, where $c_{\rm g} \equiv \frac{(f-2)^{f-2}}{(f-1)^{f-1}}$ is a threshold value representing the gel point.

The pattern of solution can be summarized as follows. For fixed density ρ_0, increasing $\lambda_{\rm b}$ amounts to increasing p_0. Below the gel point $p_0 = \frac{1}{f-1}$, the value of c also increases. For

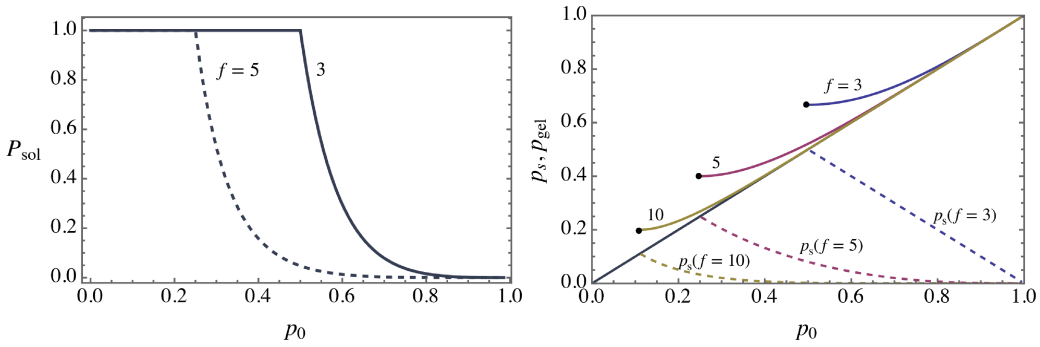

Figure 2: Left: Fraction of sol chains versus the mean-field reaction conversion for $f = 3$ and 5. Right: bonding probabilities for *gel* chains (solid) and *sol* chains (dashed) at different f. The diagonal line is the limiting behavior for $f = \infty$. The dots indicate the mean-field gel point $\frac{1}{f-1}$.

each value, two solutions of eq. (26) can be found and the *smaller* one is the physical solution, which we denote x_0. At the gel point, $c = c_{\rm g}$ and $x = x_{\rm g} \equiv \frac{f-1}{f-2}$. Above the gel point, the value of coefficient c decreases with p_0 and, again, two solutions are found, with the physical one x_0 now being the *greater* ($x_0 > x_{\rm g}$). This physical solution contains contributions from both the *sol* and *gel* chains.

The smaller solution above the gel point, which decreases monotonically as p_0 increases, corresponds to the finite clusters belonging to the *sol* phase. Denoting this solution by $x_{\rm s}$, the density of *sol* chains is given by $\int {\rm d}s\, \phi_{\rm s}^*(s)\phi_{\rm s}(s)$. In section S1.1, we show that the ratio of this density and the total segmental density, i.e. the order parameter, can be written

$$P_{\rm sol} = \left[(1-p_0)\phi_{\rm s}^*(0)\tau^{-1}\right]^f \tag{27}$$

in which $\phi_{\rm s}^*(0)$ is obtained from $x_{\rm s}$. The curves in Fig. 2 are generated using the above expression. Substituting $x_{\rm s} = P_{\rm sol}^{1/f}(1-p_0)^{-1}$ into eq. (26), we obtain

$$P_{\rm sol}^{1/f} = (1-p_0) + p_0 P_{\rm sol}^{(f-1)/f} \tag{28}$$

When expressed in terms of $P_{\rm sol} = 1 - P_{\rm gel}$, the above equation is known as the equation of the gel curve.[34] The factor $P_{\rm sol}^{1/f}$ gives the probability that the end of a randomly selected arm

is not connected to the gel network, which is decomposed into two contributions. The first is the probability that the selected end is not bonded, $1-p_0$. The second is the probability that the selected end is bonded, but is not further connected with gel network via the other $f-1$ arms on the same star, $p_0 P_{\rm sol}^{(f-1)/f}$. Equation (28) is identical to eq. (6.51) of Rubinstein and Colby's text.[34] In essence, what we have demonstrated is that the iterative argument adopted in the FS theory coincides with the saddle point condition for the field theory. The order parameter $P_{\rm sol}$ is the generating function for the number of finite clusters. When $P_{\rm sol}$ is Taylor-expanded in powers of p_0 using eq. (28), the coefficient of p_0^s is the fraction of stars in tree-like clusters containing s stars. This property can be used to evaluate $N_{\rm n}$, $N_{\rm w}$ and higher order of moments.

Over the full range of p_0, the chemical potential of stars is given by eq. (21), which decreases progressively with p_0 for constant overall segmental density ρ_0 and interaction strength u_0. Section S1.1 shows that the clusters formed from the *sol* chains above the gel point have the same chemical potential, which justifies the assignment of the solution $x_{\rm s}$ to the *sol* chains and equilibrium between finite clusters and *gel*-strands. The *sol* chains exhibits on average a bonding probability $p_{\rm s}$, which is related to $x_{\rm s}$ through $x_{\rm s} = \frac{1}{1-p_{\rm s}}$. This probability is less than the bond conversion p_0 for the whole system. Therefore, the bonding probability for the *gel* chains must be above p_0, which can be calculated using the conservation of total bond number as $\frac{p_0 - p_{\rm s} P_{\rm sol}}{P_{\rm gel}}$. The variation of $p_{\rm s}$ and bonding probability of the *gel* chains are shown in Fig. 2b. As the gel point is approached, the bonding probability $p_{\rm gel}$ has the limiting value $\frac{2}{f}$ and $P_{\rm gel}$ drops to zero. The limiting value $p_{\rm gel} = \frac{2}{f}$ corresponds to the minimum bonding probability at which tree-like products can become infinite clusters as each chain in the cluster will on average propagate the cluster. Above the gel point, the system can be considered *topologically* heterogeneous, even while remaining *spatially* homogeneous. The *gel* network that percolates the system volume is impregnated with finite clusters that have a broad size distribution and smaller bond conversion $p_{\rm s}$. Next, we turn to see under what conditions gelation can be accompanied by phase separation.

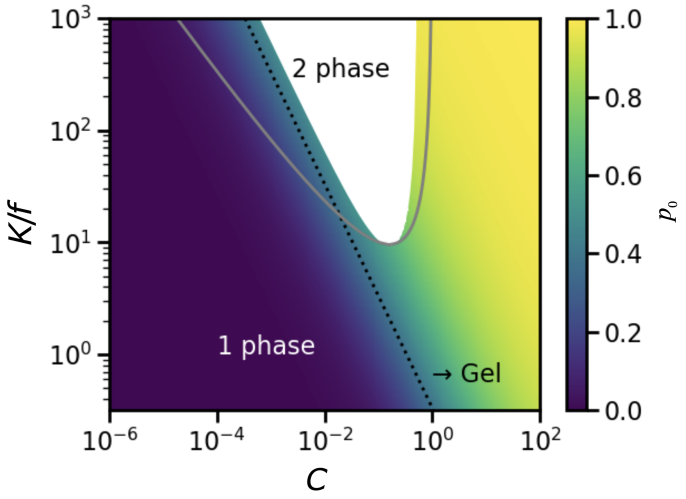

Figure 3: Universal mean-field phase diagram for end-linking star polymers with $f = 3$ arms. The binodal is indicated with the grey curve whereas the spinodal region is indicated with white. The black line is the gel transition. The background of the plot is colored according to the conversion of end groups p_0. Parameters: $C = \rho_0 u_0 N f$; $K = \lambda_b/(u_0 N^2 f)$.

3.3 Phase separation vs. gelation

Using the mean-field expressions for the osmotic pressure and the chemical potential, we can identify the condition of phase separation and the equilibrium concentrations of the coexisting dilute and concentrated phases. For fixed molecular parameters N and f, the thermodynamic state can be parameterized by the dimensionless concentration $\rho_0 u_0$ and dimensionless reactivity λ_b/u_0. In fact, it is evident from eqs. (20) and (21), that the scaled osmotic pressure $u_0\Pi_0$ and the shifted chemical potential $\mu + \ln(u_0/v)$ depend on the dimensionless combinations, $\rho_0 u_0$ and p_0, whereas the bonding probability p_0 depends on $\rho_0\lambda_b$, which can be factored into the product $(\rho_0 u_0)(\lambda_b/u_0)$.

In Fig. 3 we present the phase diagram for $f = 3$ in the coordinates of the reduced concentration $C \equiv \rho_0 u_0 N f$ and reduced reactivity $K \equiv \lambda_b/(u_0 N^2 f)$. The grey curve denotes the binodal in the system, whereas the white region is the interior of the spinodal determined using eq. (25). The dotted black line indicates the Flory gel point which is computed according to $p_0 = \frac{1}{f-1}$. Plugging this condition into eq. (19), it is straightforward to see that the mean-field gelation line is given by $CK = \frac{f-1}{(f-2)^2}$. This is an underestimate of

the true gel point since the formation of loops is not accounted for at the mean-field level. Fig. 3 can be compared with the analogous mean-field theory prediction for linear associative polymers.[29]

The figure shows that at small values of λ_b/u_0, i.e., weak bonding or good solvent quality, the system does not undergo phase separation for any concentration of polymer. It can still undergo gelation for sufficiently concentrated solutions, however. For large λ_b/u_0, a two phase region occurs. Notably, the spinodal for this region lies entirely in the gel regime. This has important implications for experimental studies depending on how the system is prepared, since the system could first percolate to form a network before undergoing phase separation. This would significantly hinder the kinetics of phase separation. Because the bonds are reversible, at sufficiently long times the system will be able to fully phase separate, but large scale separation could be suppressed for a considerable amount of time if λ_b/u_0 is large. The physical interpretation of the phase coexistence region is that the equilibrium constant is sufficiently large such that the system wants to form a gel, however, the concentration is low enough that the polymers would have to stretch excessively to reach one another to maintain a homogeneous solution. Instead, the system phase separates into a concentrated polymer phase that can easily form a gel and a sol phase where polymers are sufficiently dilute that they do not form a network. This phenomenon is often referred to as syneresis. It should be noted that Fig. 3 is constructed using the mean-field theory, which neglects loop formation. In sec. 5.3 below, we will discuss the possibility that loop formation delays or eliminates the gel point in the dilute region.

In addition to the equilibrium constant λ_b and concentration ρ_0, the excluded volume parameter u_0 is a measure of the solvent quality and is non-negative for theta and good solvents. As the the solvent quality increases (larger u_0), polymer chains undergo coil expansion and the arms of the star will stretch out. This increases the pervaded volume of each molecule and the number of molecules that each polymer can interact with will increase. The grouping $\rho_0 u_0$ thus represents this effective concentration that is increased by solvent quality. On the

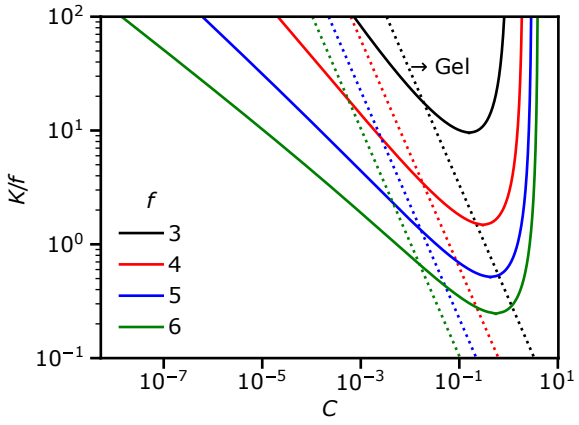

Figure 4: Mean-field phase diagram for end-linking star polymers for a variety of number of arms f. Binodals are indicated with solid lines while dotted lines indicate the gel transition. Parameters: $C = \rho_0 u_0 N f$; $K = \lambda_\mathrm{b}/(u_0 N^2 f)$.

other hand, when the solvent quality is high, polymer would rather be surrounded by solvent molecules than other polymer segments. This means that forming a supramolecular bond will be energetically disadvantageous for large u_0. As such, the effective bond strength λ_b/u_0 is reduced and bond formation is suppressed.

The effect of the arm number f on the phase behavior is illustrated in Fig. 4. As the number of arms is increased, the binodal shifts to lower values of K as do the gel transition curves. For larger number of arms it is easier to undergo gelation as a smaller conversion is required to percolate the system, so smaller values of λ_b (or ρ_0) are required for gelation. Similarly, increased f expands the regime in which gelation is favorable, but not possible due to insufficient polymer concentration, so the binodal regions shift to lower λ_b as well. Although not shown in Fig. 4, the spinodal for each value of f lies completely in the gel region.

For each f value, a critical point can be identified at the minimum value of K on the spinodal curve, the latter depending on K implicitly via p_0. By setting $\frac{\mathrm{d}K}{\mathrm{d}C} = 0$ for solution of the spinodal condition eq. (25) and applying eq. (23) to carry out the chain rule, we show

in section S1.2 that the value of p_0 at the critical point satisfies

$$f = \frac{(1+p_0)^3}{p_0^2\,(3+p_0)} \tag{29}$$

which agrees to the expression obtained by Semenov and Rubinstein for associative linear polymers.[29] Equation (29) has a unique positive root between 0 and 1 for $f \geq 2$ and decreases monotonically from $p_0 = 1$ at $f = 2$ to 0 at large f. For the example of $f = 3$, we have $p_0 = 0.63$. By plugging eq. (29) into eq. (25) to eliminate f, the value of C at the critical point is found to be $\frac{1-p_0}{p_0(3+p_0)}$. Correspondingly, the value of K is calculated from eq. (19). By eliminating p_0 from expressions for C and K, a quadratic equation in K is obtained in section S1.2, whose solution approaches $K = \frac{1+6C}{16C^3}$ for small C and approaches $K = \frac{1}{3C^2}$ for large C. As f is increased from $f = 2$, the critical point moves from $C = 0$ and $K = \infty$ towards the lower right corner of Fig. 4. In the limit of large f, the solution for p_0 approaches $\frac{1}{\sqrt{3f}}$, and correspondingly, C approaches $\sqrt{\frac{f}{3}}$ and K approaches $\frac{1}{f}$.

The mean-field analysis provides a comprehensive and thermodynamically consistent picture of phase separation and gelation, but a few inherent problems should be noted. Firstly, it neglects the presence of any rings or loops in the system and assumes that only tree-like products are possible.[37] Such a picture of gelation is unphysical, especially at low concentrations where intramolecular bonds (producing only loops) are more probable than intermolecular bonds. Additionally, the mean field predictions neglect all concentration fluctuations in the system which will simultaneously influence the reaction equilibria, the gelation behavior, and phase separation. A preliminary analyses of these issues at the Gaussian fluctuation level will be presented in the following sections.

4. Loop density in fluctuation theory

A major deficiency of the mean-field theory is the omission of cyclic polymer structures, which focuses on the tree-like clusters, e.g., Fig. 1b,c. Although our primary concern in this

work is the presentation of the Gaussian fluctuation theory, it will be important to assess to what degree it restores cyclic structures relevant to gelation and phase separation behavior. For this reason, it is essential that we have tools for exactly counting the number of loops present in a reacting system. In this section, we first summarize a well-known topological result that relates the loop density to the densities of polymers, bonds, and stars, then cast it in the form of fluctuation corrected quantities. Next, we introduce a loop density operator that permits direct enumeration of loops. Both sets of results are valid generally, and will be specifically applied with the added approximation of Gaussian fluctuations in the subsequent section. Examples of loop-containing clusters are provided in Fig. 1d–h.

4.1 Topological constraint

The densities of loops $\rho_{\rm l}$, arm ends $\rho_{\rm e}$, polymers (or clusters) $\rho_{\rm p}$, and f-arm stars ρ_f, in an arbitrary ensemble of associated species are related by a topological constraint. This is the Euler relation adapted to the problem of polymer gelation by Lubensky and Isaacson:[7,8]

$$\begin{aligned}\rho_{\rm p} &= \rho_{\rm l} + \frac{1}{2}\,\rho_{\rm e} + (1-f/2)\,\rho_f \\ &= \rho_{\rm l} + \frac{\rho_0}{2N}(1-p) + (1-f/2)\,\frac{\rho_0}{fN}\end{aligned} \tag{30}$$

In the second line, the end density $\rho_{\rm e}$ is expressed using the arm number density $\frac{\rho_0}{N}$ and the fraction of non-reacted ends $1-p$. The star number density ρ_f has also been expressed in terms of the monomer density ρ_0. At the mean-field level, $\rho_{\rm l}=0$, the above relation reduces to the Carothers equation[33] for the number average molecular weight, $N_{\rm n} = \frac{\rho_0}{\rho_{\rm p}} = \frac{fN}{1-pf/2}$. To discuss the fluctuation correction, it is convenient to hold the monomer number density ρ_0 fixed, and focus on the variational form of the Euler relation,

$$\delta\rho_{\rm p} = \rho_{\rm l} - \frac{\rho_0}{2N}\delta p = \rho_{\rm l} - \delta\rho_{\rm b} \tag{31}$$

Here the variation is defined in reference to the mean-field solution where $\rho_{\rm l} = 0$. In the variational expression above we use $\rho_{\rm l}$ rather than $\delta\rho_{\rm l}$ due to the zero reference value. The combination $\frac{\rho_0}{2N}\delta p$ is recognized as the variation of the bond density $\delta\rho_{\rm b}$. It is seen that forming loops increases the number of polymers, whose effect is opposite to that of bond formation. In the analysis below, we can focus on the two independent variables $\rho_{\rm l}$ and $\delta\rho_{\rm b}$.

The variation in bond number density is derived by differentiating the fluctuation free energy or minus the fluctuation correction to the osmotic pressure $\Delta\Pi$ with respect to the bond chemical potential $\mu_{\rm b} \equiv \ln\lambda_{\rm b}$ (see eq. (10)):

$$\delta\rho_{\rm b} = \frac{\partial p_0}{\partial\mu_{\rm b}}\frac{\partial\Delta\Pi}{\partial p_0} = \frac{p_0(1-p_0)}{1+p_0}\frac{\partial\Delta\Pi}{\partial p_0} \tag{32}$$

In the last step, the relation $\frac{\partial p_0}{\partial\lambda_{\rm b}} = \frac{p_0(1-p_0)}{\lambda_{\rm b}(1+p_0)}$ was inserted, which is derived from eq. (19) for the law of mass action, $\frac{p_0}{(1-p_0)^2} = \frac{\rho_0}{N}\lambda_{\rm b}$.

Our approach to calculating the loop number density $\rho_{\rm l}$ is indirect. We first develop an operator for the total polymer density $\rho_{\rm p}$ and then use the Euler relation eq. (30) to solve for $\rho_{\rm l}$ given that we already have exact operator expressions for $\rho_{\rm e}$ and ρ_f. Here we sketch the approach and provide the main result, leaving the detailed derivation to the subsequent section.

To count the number of polymers, we note that each polymer is a *connected* cluster and, if the clusters are *non-interacting*, each is subject to free translation and contributes a factor V to the partition function. A configuration containing $n_{\rm p}$ non-interacting polymers therefore contributes a factor $V^{n_{\rm p}}$ to the partition function. Differentiating the logarithm of the partition function with respect to the logarithm of volume V therefore gives the average number of polymers $\langle n_{\rm p}\rangle$. Real polymers are of course interacting, but in the CST partition function it is the w integral that installs the pairwise interactions. Thus if the V derivative is taken *before* the w average is performed, we can derive an operator for the average number of polymers. The next subsection shows that this procedure leads to the polymer number

density $\rho_{\rm p} = \frac{\langle n_{\rm p}\rangle}{V}$ decomposed into the same form as eq. (30):

$$\rho_{\rm p} = \rho_{\rm l} + \frac{1}{2}\rho_{\rm e} + (1 - f/2)\,\rho_f \tag{33}$$

Here the respective densities are given by

$$\rho_{\rm l} = -\frac{b^2}{9V}\int {\rm d}s \int {\rm d}\mathbf{r}\, \left\langle \phi^*(\mathbf{r}, s)\nabla^2\phi(\mathbf{r}, s)\right\rangle \tag{34}$$

$$\rho_{\rm e} = \frac{1}{V}\int {\rm d}\mathbf{r}\, \left\langle \phi(\mathbf{r}, N)\right\rangle \tag{35}$$

$$\rho_f = \frac{\lambda_f}{f!V}\int {\rm d}\mathbf{r}\, \left\langle \phi^*(\mathbf{r}, N)^f\right\rangle \tag{36}$$

The expressions for ρ_f and $\rho_{\rm e}$ are identical to eqs. (9) and (11), with $\rho_{\rm e}$ being simply related to $\rho_{\rm b}$. The operator for the loop number density $\rho_{\rm l}$, eq. (34), is a new result. Because of the Laplacian operator, it is clear that the mean-field solution with homogeneous CST field values does not contribute to the average in eq. (34). Spatial variation or fluctuation in the CST fields is needed to describe loops.

4.2 Loop density operator

Next we provide a more detailed sketch of the derivation of this result for the loop density operator. The partition function in eq. (1) contains two field integrals, the outer one over the auxiliary field w and the inner one over the CST fields ϕ and ϕ^*. The inner CST integral has two important properties. First, for fixed $w(\mathbf{r})$ field, all bonding patterns are enumerated by the integral over the ϕ and ϕ^* fields. Second, the stars and the resulting polymers are non-interacting until the outer w integral is performed. When the Boltzmann factor ${\rm e}^{-H[\phi,\phi^*,w]}$, excluding the term $H_w \equiv \frac{1}{2u_0}\int {\rm d}\mathbf{r}\, w^2$, is Taylor-expanded and integrated over the CST fields, the surviving terms are a mix of connected clusters. Each cluster represents one polymer with certain crosslinking structure and contributes a value proportion to V, due to the spatial translation. A configuration with $n_{\rm p}$ clusters or polymers contributes a factor $V^{n_{\rm p}}$ to the

partition function.

Therefore, the average polymer number can be obtained from

$$\begin{aligned}\langle n_{\rm p}\rangle &= \int \frac{\mathcal{D}[w]}{D_w} {\rm e}^{-H_w} \frac{\partial \ln \Xi_\phi}{\partial \ln V} \\ &= \left\langle \frac{\partial \ln \Xi_\phi}{\partial \ln V} \right\rangle_w \end{aligned} \tag{37}$$

where the partition function for the CST fields subject to the fixed AF field w is defined as

$$\Xi_\phi = \int \frac{\mathcal{D}[\phi,\phi^*]}{D_\phi}\, {\rm e}^{-H[\phi,\phi^*,w]+H_w} \tag{38}$$

The notation $\langle\cdot\rangle_w$ indicates an average weighted by $\exp(-H_w)$. Introducing the analogous notation $\langle\cdot\rangle_\phi$ for an average weighted by a Boltzmann factor with the CST Hamiltonian $H_\phi \equiv H[\phi,\phi^*,w] - H_w$, the polymer number density $\rho_{\rm p} = \langle n_{\rm p}\rangle / V$ can be written as

$$\rho_{\rm p} = \frac{\langle n_{\rm p}\rangle}{V} = \left\langle \left\langle -\frac{\partial H_\phi}{\partial V} \right\rangle_\phi \right\rangle_w \tag{39}$$

where we have assumed that the normalizing denominator D_ϕ has no volume dependence. This can be achieved by rescaling the spatial coordinates and fields as follows: $\mathbf{r} = \mathbf{x}V^{1/3}$, $\bar{\phi}(\mathbf{x},s) = V^{1/2}\phi(\mathbf{r},s)$ and $\bar{\phi^*}(\mathbf{x},s) = V^{1/2}\phi^*(\mathbf{r},s)$. Then we find that H_ϕ can be written as the sum of

$$-\frac{b^2}{6}V^{-2/3}\int {\rm d}s \int {\rm d}\mathbf{x}\, \bar{\phi^*}\nabla^2_{\mathbf{x}}\bar{\phi} - V^{1-f/2}\frac{\lambda_f}{f!}\int {\rm d}\mathbf{x}\, \bar{\phi^*}(\mathbf{x},0)^f - V^{1/2}\int {\rm d}\mathbf{x}\, \bar{\phi}(\mathbf{x},N) \tag{40}$$

in addition to two terms that are independent of V: one from the reaction term $\phi(\mathbf{x},N)^2$ and one from the coupling with the auxiliary potential w. Differentiation of H_ϕ, followed by restoring the $\mathbf{r}$ coordinate and fields gives

$$\frac{\partial H_\phi}{\partial V} = \frac{b^2}{9V}\int {\rm d}s \int {\rm d}\mathbf{r}\, \phi^*\nabla^2\phi - \frac{(1-f/2)\lambda_f}{f!V}\int {\rm d}\mathbf{r}\, \phi^*(\mathbf{r},0)^f - \frac{1}{2V}\int {\rm d}\mathbf{r}\, \phi(\mathbf{r},N) \tag{41}$$

Substituting the above back to eq. (39) leads to

$$\rho_{\rm p} = \rho_{\rm l} + (1 - f/2)\rho_f + \frac{1}{2}\rho_{\rm e} \tag{42}$$

which coincides with the topological relation, eq. (30) with the three densities taking the forms given in eqs. (34–36). In particular, applying eq. (34) to diagrams in Fig. 1a–g results in loop counts $0, 0, 0, 1, 1, 1, 3$, and 2 respectively.

It is natural to ask how the particular form of the loop density operator counts loops. To see this, we need to examine the effects of the operator $-\phi^*(\mathbf{r}, s)\nabla^2\phi(\mathbf{r}, s)$ applied to individual polymers. In section A2, we show that applying the loop operator to a polymer generates a result equal to the sum of the compression factors of *all* the arms in the polymer, divided by the volume V. The compression factor is defined as the average

$$\langle\varsigma\rangle = 1 - \frac{\langle\mathbf{r}^2\rangle}{R^2} \tag{43}$$

where $\mathbf{r}^2$ is the end-to-end vector of the arm under consideration, and $R^2 = Nb^2$ is the unperturbed Gaussian value. The average $\langle\cdot\rangle$ is evaluated for the non-interacting stars under the fixed potential w.

The compression factor is non-vanishing only if the arm is part of a loop. If it belongs to a dangling end or a part of a tree diagram, the average $\langle\mathbf{r}^2\rangle = R^2$ because the conformational statistics of the arm is not constrained. However, if the arm is part of, say, a simple loop consisting of n arms, the distribution of the end-to-end vector $\mathbf{r}$ is constrained by the arm itself, which is Gaussian with variance $Nb^2/3$, and by the complementing $(n-1)$ arms, which is Gaussian with variance $(n-1)Nb^2/3$. The constraint of two Gaussian strands producing $\mathbf{r}$ vectors simultaneously, reduces the average to $\langle\mathbf{r}^2\rangle = (1-1/n)Nb^2$. As a result, the compression factor of one arm in the simple loop is $1/n$. The sum over the n arms involved gives the correct counting of one loop which, when normalized by the volume V, gives the loop number density. Physically, what we observe is the natural expectation that

each arm belonging to a loop is slightly compressed, and the sum of compression factors counts the loops.

5. Gaussian fluctuation theory

Our approach to assessing fluctuations in the CST assumes that the system fluctuates around the homogeneous saddle point and that the magnitude of these fluctuations are small. This allows expansion of the Hamiltonian around the saddle point state and truncation at quadratic order, yielding a set of Gaussian functional integrals that can be performed analytically. Throughout this section, such fluctuation analysis is carried out below the mean-field gel point, in close vicinity of the saddle point for the *sol* phase.

5.1 RPA free energy

The FS theory addresses the statistics of tree-like clusters formed by arm association. To incorporate the effects of loops as well as excluded volume correlations, we examine the nature of Gaussian fluctuations in both the CST fields and the auxiliary field. Around the spatially homogeneous saddle point, the small fluctuations are parameterized as follows,[25]

$$\begin{aligned} \phi^*(\mathbf{r}, s) &= \phi_0^*(s)(1 + \psi^*(\mathbf{r}, s)) \\ \phi(\mathbf{r}, s) &= \phi_0(s)(1 + \psi(\mathbf{r}, s)) \\ \mathrm{i}w(\mathbf{r}) &= \omega_0 + \omega(\mathbf{r}) \end{aligned} \tag{44}$$

To simplify the notation, we have absorbed the imaginary unit i into ω_0 and $\omega(\mathbf{r})$. The perturbations $\psi(\mathbf{r}, s)$, $\psi^*(\mathbf{r}, s)$ and $\omega(\mathbf{r})$ are understood to be small and of similar amplitude. The minimal order of fluctuation correction is obtained by substituting these expressions into the Hamiltonian and expanding it to quadratic order in the fluctuation fields, which can be conveniently done in Fourier space. Our convention for forward and inverse Fourier

transforms, using $\omega(\mathbf{r})$ as example, is $\hat{\omega}_{\mathbf{k}} = \int \mathrm{d}\mathbf{r}\, \mathrm{e}^{-\mathrm{i}\mathbf{k}\cdot\mathbf{r}}\omega(\mathbf{r})$ and $\omega(\mathbf{r}) = \frac{1}{(2\pi)^3}\int \mathrm{d}\mathbf{k}\, \mathrm{e}^{\mathrm{i}\mathbf{k}\cdot\mathbf{r}}\hat{\omega}_{\mathbf{k}}$.

The coefficients for the other field variables, in particular $\hat{\psi}_{\mathbf{k}}(s)$ and $\hat{\psi}^*_{\mathbf{k}}(s)$ are similarly defined. The transform of the delta function $\delta(\mathbf{r})$ is $\hat{\delta}_{\mathbf{k}} = 1$. So we can use $\int \mathrm{d}\mathbf{k}\, \mathrm{e}^{\mathrm{i}\mathbf{k}\cdot\mathbf{r}} = (2\pi)^3\delta(\mathbf{r})$ and $\int \mathrm{d}\mathbf{r}\, \mathrm{e}^{\mathrm{i}\mathbf{k}\cdot\mathbf{r}} = (2\pi)^3\delta(\mathbf{k})$ to facilitate the forward and inverse transforms. For instance, this enables us to write $\int \mathrm{d}\mathbf{r}\, \psi(\mathbf{r},s)\omega(\mathbf{r}) = \int \frac{\mathrm{d}\mathbf{k}}{(2\pi)^3}\, \hat{\psi}_{\mathbf{k}}(s)\hat{\omega}_{-\mathbf{k}}$, as an example of Parseval's theorem.[38] A further simplification we shall use below is $\hat{\omega}_{-\mathbf{k}} = \hat{\omega}_{\mathbf{k}}$ because of the inversion symmetry around the homogeneous solution. The units of the relevant amplitudes for field variable fluctuations are: $[\omega(\mathbf{r})] = [\psi(\mathbf{r},s)] = [\psi^*(\mathbf{r},s)] = 1$ and $[\hat{\omega}_{\mathbf{k}}] = [\hat{\psi}_{\mathbf{k}}(s)] = [\hat{\psi}^*_{\mathbf{k}}(s)] =$ volume. For consistency, the accent $\hat{}$ is reserved for Fourier mode amplitudes.

In section S3, we show that the quadratic contributions to the Hamiltonian from a given $\mathbf{k}$ mode equals the product of the arm number density ρ_0/N and the following,

$$\int \mathrm{d}s\, \hat{\psi}^*_{\mathbf{k}}(s)\, \mathcal{L}\, \hat{\psi}_{\mathbf{k}}(s) + \int \mathrm{d}s\, \big[\hat{\psi}_{\mathbf{k}}(s) + \hat{\psi}^*_{\mathbf{k}}(s)\big]\hat{\omega}_{\mathbf{k}} - \frac{f-1}{2}\hat{\psi}^*_{\mathbf{k}}(0)^2 - \frac{p_0}{2}\hat{\psi}_{\mathbf{k}}(N)^2 - \frac{N}{2\rho_0 u_0}\hat{\omega}^2_{\mathbf{k}} \quad (45)$$

In $\mathbf{k}$ space, the ideal chain evolution operator is $\mathcal{L} = \frac{\partial}{\partial s} + \frac{b^2}{6}\mathbf{k}^2$. The above quadratic form is amenable to standard Gaussian analysis, which yields the Gaussian or RPA grand potential and the corresponding Gaussian fluctuation correction to the osmotic pressure,

$$\begin{aligned}\Pi_{\mathrm{G}} = \frac{1}{V}\ln \Xi_{\mathrm{G}} &= -\frac{1}{2}\int \frac{\mathrm{d}\mathbf{k}}{(2\pi)^3} \ln\Big(\hat{\Delta}(1+\rho_0 u_0 N\hat{G})\Big) \\ &\equiv \Pi_{\mathrm{G,l}} + \Pi_{\mathrm{G,v}} \end{aligned} \quad (46)$$

The total osmotic pressure is given by the sum of Π_{G} and the mean-field contribution, $\Pi = \Pi_0 + \Pi_{\mathrm{G}}$. Equation (46) includes contributions from different Fourier modes. The term $\hat{\Delta}(x) \equiv 1 - p_0(f-1)\mathrm{e}^{-2x}$, with $x \equiv k^2 N b^2/6$, will be seen to be derived from clusters that contain a single loop. The term $\hat{G}$ is the RPA structure factor for a mixture of tree-like

clusters resulting from star association,

$$\hat{G} \equiv \hat{g}(x) + \hat{h}(x)^2 \frac{(f-1) + p_0 + 2p_0(f-1)\mathrm{e}^{-x}}{1 - p_0(f-1)\mathrm{e}^{-2x}} \tag{47}$$

where $\hat{g}(x) \equiv \frac{2}{x^2}(x - 1 + \mathrm{e}^{-x})$ is the Debye function, and $\hat{h}(x) \equiv \frac{1}{x}(1 - \mathrm{e}^{-x})$.

The definition in the last line of eq. (46) assigns the terms derived from $\ln \hat{\Delta}$ and $\ln(1 + \rho_0 u_0 N \hat{G})$ to $\Pi_{\mathrm{G,l}}$ and $\Pi_{\mathrm{G,v}}$ that represents contributions due to loop formation and excluded volume correlations respectively. The advantage of this decomposition will be justified by noticing that $\Pi_{\mathrm{G,l}}$ provides the only RPA contribution to the loop density, and $\Pi_{\mathrm{G,v}}$ depends on the excluded volume interaction. Notably, in the case of no reactions, $p_0 = 0$, so no loops are possible and $\Pi_{\mathrm{G,v}}$ recovers the RPA fluctuation contribution to the free energy for a solution of interacting homopolymer stars.

The above free energy expression is our main result. The underlying algebraic details are provided in section S3, and the physical implications will be our main concern in the sections below. Here we note that the types of fluctuations considered are those around the *fixed* homogeneous mean-field saddle point, which does not shift the total segmental number density. So a treatment in the GCE or CE yields identical results and the parameterization using p_0 and ρ_0 is both intuitive and convenient.

The RPA free energy can be independently derived by a diagrammatic expansion. In section S4, we show explicitly that the RPA free energy can be constructed by two groups of diagrams (Fig. S3, SI). The first group captures excluded volume correlations among tree clusters. The second group contains single loops, which belongs to the category of the diagrams on the right side of Fig. S2 (SI). Therefore, applying the loop density operator, eq. (34), to each diagram in this group results in a count of one. The sum of statistical weights of the diagrams in group 2 normalized by volume V gives the loop density, which is

precisely $\Pi_{\mathrm{G,l}}$. At the Gaussian level, we can write

$$\rho_{\mathrm{l}} = \Pi_{\mathrm{G,l}} = -\frac{1}{2}\int \frac{\mathrm{d}\mathbf{k}}{(2\pi)^3} \ln \hat{\Delta} = \left(\frac{3}{4\pi}\right)^{3/2} \frac{\mathrm{Li}_{5/2}(z)}{2R^3} \tag{48}$$

in which $\mathrm{Li}_{5/2}(z)$ with $z \equiv p_0(f-1)$ is the poly-log function defined by the sum $\mathrm{Li}_n(z) = \sum_{k=1}^{\infty} \frac{z^k}{k^n}$. The types of loops sketched in Fig. 1d–g, which are isolated simple ones, are included by eq. (48), but the loops of the type Fig. 1h or more complicated ones are not included at the Gaussian level. We stress that this expression gives the correct loop density at the Gaussian level regardless of the concentration and the interaction strength. The difference among the examples discussed below arises solely from the variation in bond density $\delta\rho_{\mathrm{b}}$.

5.2 Structure factor

To understand the physical meaning of the RPA structure factor $\hat{G}$, we recall that each tree diagram is just a connected portion of the infinite Bethe lattice.[39] From each lattice site grows f arms outwards. The crosslinking is represented by connecting the ends of two arms, with probability p_0. To generate the ensemble of clusters, one starts from an arbitrary arm on *any* star (the choice of star does not matter since all stars on the Bethe lattice are equivalent statistically), and walks to the end of this arm, or to the end of the remaining $f-1$ arms. At any of these f ends, the star connects with probability p_0 to some other star. Below the percolation threshold $\frac{1}{f-1}$, all finite tree clusters are produced by iteration. Because all arms are statistically equivalent on the Bethe lattice, instead of enumerating all stars, we may calculate the structure function on the Bethe lattice itself, by noticing that the structure factor is a measure of the correlation between two randomly selected arms on the Bethe lattice. Our iterative derivation of the structure factor is similar to those adopted in the literature.[40,41]

We therefore proceed as follows. First, label a randomly selected arm on a Bethe lattice 1

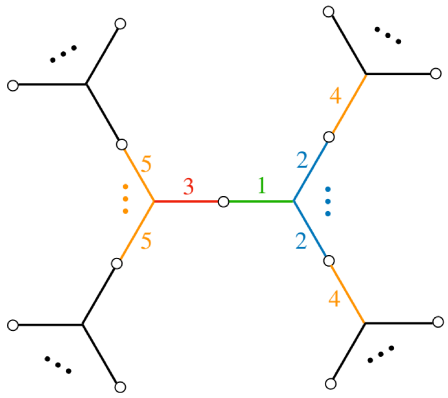

Figure 5: Illustration of the recursive nature for RPA structure factor. The numerals indicate the "distance" on the Bethe lattice from a randomly selected initial arm labeled 1.

(Fig. 5), to which $f-1$ arms living on the same star are linked and labeled 2. Another arm labeled 3 may be linked to 1 with probability p_0, with which $f-1$ arms labeled 5 belong to the same star. Similarly, with probability p_0, each of the arms labeled 2 may be crosslinked to one of the $f-1$ arms labeled 4. This whole cascading process propagates indefinitely. For ease of tracking, we call arm 1 generation 1, arms $2, 3, 4, 5$ generation 2, etc. The generation is defined by either encountering a new crosslinking site that demands a probability p_0 to advance further (e.g., ends of arms 5), or by encountering a new branching point (e.g., ends of arms 4 that meets the star centers). Therefore, every generation grows *two* bonds outwards.

To calculate the pair correlation, our strategy is to consider the correlation between arm 1 and all the generations produced via the iterative procedure. The self-correlation $(1-1)$ is the Debye function $\hat{g}(x)$. The contributions from generation 2 are given by

$$\left[(f-1) + p_0 + 2p_0(f-1)\mathrm{e}^{-x}\mathrm{e}^{-x}\right] \hat{h}(x)^2 \tag{49}$$

These correlations have the common factor $\hat{h}(x)^2$. The coefficients in the brackets correspond to correlations $(1-2)$, $(1-3)$, and equal contributions from correlations $(1-4)$ and $(1-5)$. The contributions from generation 3 equals $p_0(f-1)\mathrm{e}^{-2x}$ times that of generation 2, and those from each higher order generations acquires the same additional multiplying factor. Overall, the results from generations 2 onward form a geometrical series, which combined

with the self-correlation gives

$$\hat{G} = \hat{g}(x) + \hat{h}(x)^2 \frac{(f-1) + p_0 + 2p_0(f-1)\mathrm{e}^{-x}}{1 - p_0(f-1)\mathrm{e}^{-2x}} \tag{50}$$

The second term is recognized as eq. (49) divided by $\hat{\Delta}$, which captures the correlations between distinct arms on the same cluster averaged over the cluster population.

The above result for $\hat{G}$ can be interpreted as the structure factor for an ensemble of tree-like clusters following the FS statistical weight. In the absence of cross-linking, with $p_0 = 0$, it reduces to the structure factor of a single star, $\hat{g}(x)+(f-1)\hat{h}(x)^2$, in which $(f-1)$ obviously counts the neighboring arms on the same star. For non-zero p_0, the expression is simplified in the limit of large N. We can drop all the exponential terms and obtain $\frac{2}{x} + \frac{-2+(f-1)+p_0}{x^2}$. The leading term is the Edwards approximation to the intra-arm correlation. The secondary term contains a variety of end correlations: those from ends on the same arm (-2), that from arm center connected to remaining arms on the same star $(f-1)$, and that from the bonded arm at the arm end (p_0). For finite arm length N, the exponential factors e^{-x} or e^{-2x} represent the weights needed by the chemical distance between arms.

In the long wavelength limit, the structure factor can be expanded to linear order in x as

$$\hat{G} = \frac{f(1+p_0)}{1 - p_0(f-1)} \left(1 - k^2\xi^2 + \cdots\right) \tag{51}$$

The prefactor equals N_w/N, the ratio between weight average molecular weight and the arm length, which quantifies the density-density correlation and can be related to the osmotic compressibility, as noted earlier. In the second factor, the correlation length ξ is found to scale as $\xi \propto R\,|\epsilon|^{-1/2}$, where $\epsilon \equiv p_0(f-1) - 1$ is the degree of gelation introduced by Flory.[34] The divergence of the correlation length is governed by the exponent $\nu = 1/2$, consistent with the prediction of mean-field theory for the gelation problem.

The structure factor $\hat{G}$ was calculated for clusters formed from non-interacting stars. When the excluded volume interaction is turned on, following the standard self-consistent

treatment,[25] it can be shown that the density response to an external perturbation $\hat{J}(\mathbf{k})$ in the linear regime is given by $\hat{\rho}_1(\mathbf{k}) = -S(k)\hat{J}(\mathbf{k})$, with $S(k)^{-1} = [\rho_0 N \hat{G}]^{-1} + u_0$. It can be expanded to $S(k)^{-1} = \frac{1}{\rho_0 N_\mathrm{w}}(1 + k^2\xi^2 + \cdots) + u_0$, whose value at $k = 0$ is identical to eq. (24). The low-k behavior of the RPA structure factor can in principle be used to obtain N_w and ξ from scattering measurements on density fluctuations conducted in the small angle regime.

5.3 Phantom stars

In the subsequent subsections, we examine the consequence of the Gaussian fluctuation by considering the densities of loops and bonds in three limiting cases. The simplest case corresponds to associative phantom stars, attained by setting $u_0 = 0$. In this limit, we have $\Pi_\mathrm{G} = \Pi_\mathrm{G,l} = \rho_\mathrm{l}$, where the loop density is given by eq. (48). Thus, the variation in bond number is entirely derived from the loop density. Substituting eq. (48) into eq. (32) yields

$$\delta\rho_\mathrm{b} = \frac{p_0(1-p_0)}{1+p_0}\frac{\partial\rho_\mathrm{l}}{\partial p_0} = \left(\frac{3}{4\pi}\right)^{3/2}\frac{1-p_0}{1+p_0}\frac{\mathrm{Li}_{3/2}(z)}{2R^3} \tag{52}$$

The polylog functions have the asymptotic behavior $\mathrm{Li}_n(z) \sim z = p_0(f-1)$ near the origin irrespective of the value of n. Therefore, in the limit of low reaction conversion, we have $\delta\rho_\mathrm{b} \propto \rho_\mathrm{l} \propto p_0(f-1)$, which implies that the variation of bond formation in the low p_0 regime is due to the formation of intra-star bonds which always produces a loop. The bond and loop densities for phantom stars, normalized by $2R^3(4\pi/3)^{3/2}$, are plotted in Fig. 6 for $f = 3, 5, 15$. In the case of $f = 3$, increasing p_0 causes the loop density ρ_l to grow faster than the variation of bond density $\delta\rho_\mathrm{b}$, which implies that inter-star bonds are suppressed in favor of intra-star bonds that form loops. For $f = 15$, the reverse is true and the variation of bond density $\delta\rho_\mathrm{b}$ grows faster than the loop density, which implies the promotion of inter-star bonds. In particular, near the gel point, most bonds associated with loop structures are inter-molecular for $f \geq 15$.

The loop density evaluated at the Gaussian level is independent of the excluded vol-

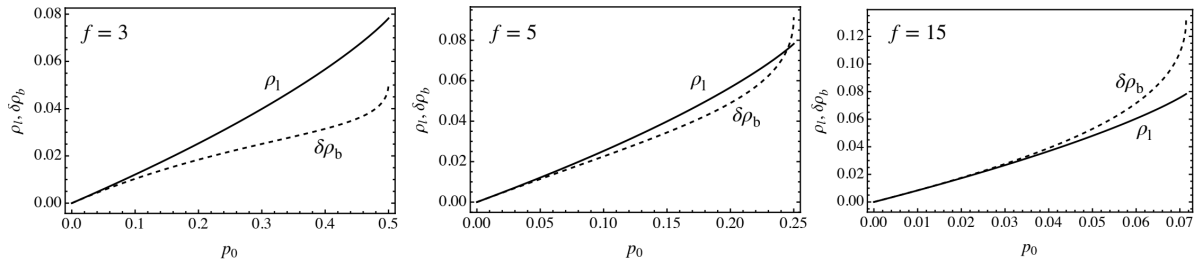

Figure 6: Variation of bond and loop densities for phantom stars with $f = 3$, 5 and 15, which are normalized by the factor $2R^3(4\pi/3)^{3/2}$. The reaction conversion is terminated at the mean-field gel point $p_0 = (f-1)^{-1}$.

ume interaction. It can be shown that our expression for the total loop density, eq. (48), generates the distribution of single loops formed via both inter- and intra-molecular bonds, which was previously considered by Jacobson and Stockmayer for linear condensation[42] and subsequently by Hoeve for f-arm stars.[43] In fact, eq. (48) can be expanded as $\rho_{\rm l} = \sum_{n=1}^{\infty} L_n$, in which

$$L_n \equiv \frac{[p_0(f-1)]^n}{2(2\pi)^3 n} \int \mathrm{d}\mathbf{k}\, \mathrm{e}^{-2nx} = \frac{1}{2}\left(\frac{3}{4\pi}\right)^{3/2} \frac{[p_0(f-1)]^n}{n^{5/2}R^3} \tag{53}$$

The term L_n is the number density of single loops constructed from n stars. The factor n^{-1} is the symmetry number of the loop, while the product $[p_0(f-1)]^n$ gives the probability of generating n bonds. The factor $(f-1)$ is included to account for the $(f-1)$ arms that may participate in loop formation. Finally, the integral over the weight e^{-2nx} gives the loop closure probability for $2n$ arms adopting Gaussian statistics, which results in additional factors of R^{-3} and $n^{-3/2}$. The most salient feature is the $n^{-5/2}$ dependence on the loop number density, initially obtained by Jacobson and Stockmayer.[42]

The simulation[44–46] and experimental[47] literature have also considered the number of loop-participating stars, which is proportional to nL_n and exhibits an $n^{-3/2}$ dependence. Specifically, the "primary" and "secondary" loops used,[46,47] are proportional to L_1 and L_2. Most of these studies considered the crosslinking formed between, for instance, A_f stars and B_g junctions. In these systems, two separate conversions conversions $p_{\rm A}$ and $p_{\rm B}$ are

needed, which are fixed by the law of mass action and mass conservation. Our expression for loop densities, eq. (53), is still applicable once $p_0(f-1)$ is replaced with $p_A p_B (f-1)(g-1)$. The predicted scaling $n^{-5/2}$ as well as the dependence on f and g is fully consistent with the simulation results,[45] which is perhaps a bit surprising. The simulations[45] use the bond fluctuation model, which contains the excluded volume interaction, while the calculation leading to eq. (53) does not address the effects of excluded volume.

In addition to fixing the necessary prefactor, equation (53) contains explicit dependence on the arm size, scaling like R^{-3}. The fraction of arms in the n-loops is given by the ratio between nL_n and the arm number density ρ_0/N. Thus the parametric combination $N/(\rho_0 R^3)$ plays an important role determining the loop density, which is consistent with the analysis of Erukhimovich,[12] the observation of Wang and Olsen et al.[46] obtained on grounds of dimensional analysis, as well as the work by Lang and Kumar.[17] Furthermore, when $R = N^{1/2}b$ is substituted, the fraction of arms forming loops scales as $N^{-1/2}$, which again is consistent with the earlier simulation data[45] and, moreover, with the expectation of the mean-field theory becoming asymptotically exact in the limit of large N.

The formation of loops delays the gel point and may, for sufficiently dilute concentration, eliminate gelation completely.[17,18,48,49] The earlier treatment of Jacobson and Stockmayer on linear polycondensation[42] shows that the reaction of telechelic chains, with $f = 2$, may result in the system containing only loops when reactivity is high. With the explicit expression for loop density L_n, we can now recapitulate their analysis for general f as follows. Since each loop of order n contains n arms, the number density of all loop-forming arms is

$$\rho_{b,l} = \sum_{n=1}^{\infty} nL_n = \left(\frac{3}{4\pi}\right)^{3/2} \frac{\mathrm{Li}_{3/2}(z)}{2R^3},$$

where $z = (f-1)p_0$ has been substituted. It is clear that $\rho_{b,l}$ increases with z. For fixed concentration ρ_0, the density $\rho_{b,l}$ reaches maximum if λ_b is on the mean-field gelation curve, giving $z = 1$. At this point, we have $\mathrm{Li}_{3/2}(1) = \zeta(3/2) = 2.61$. The Jacobson-Stockmayer

condition demands that $\rho_{\mathrm{b,l}}$ equals the number density of arms ρ_0/N. Therefore, a threshold value of segment density is identified as

$$\rho_{\mathrm{c}} = c\frac{N}{R^3},$$

where the numerical coefficient $c = \left(\frac{3}{4\pi}\right)^{3/2} \frac{\zeta(3/2)}{2} = 0.15$. The above expression for ρ_{c} is consistent with those reported in the literature.[17,18,48]

For $\rho_0 < \rho_{\mathrm{c}}$, below the threshold density, the formation of loops exhausts all arms present in the solution before the gel point is reached, making it impossible to form a gel. Apart from the numerical prefactor c, the threshold value ρ_{c} is comparable to the self-concentration of a single arm N/R^3, i.e., the crossover point between dilute and semidilute regimes. This is expected since sufficient inter-arm overlap is necessary for effective inter-molecular crosslinking. Therefore, the mean-field gelation curve identified in Section 3.3 is applicable only in the semi-dilute regime. To thoroughly discuss the impacts of loop formation, the shift to the mean-field gel point and the fluctuation effects on the bionodal diagram both need to be studied, which is beyond the scope of the current work.

5.4 Dilute solution

A second limiting case is a dilute solution of f-arm stars. The loop density can be calculated from eq. (48). The bond density variation in the dilute limit contains two contributions. The first contribution is positive, due to the formation of loops and equal to the loop density. This is verified by keeping only the linear term in $\mathrm{Li}_{5/2}(z)$ or $\mathrm{Li}_{3/2}(z)$. We have

$$\begin{aligned}\delta\rho_{\mathrm{b,l}} = \rho_{\mathrm{l}} &= \frac{p_0(f-1)}{2}\int \frac{\mathrm{d}\mathbf{k}}{(2\pi)^3}\,\mathrm{e}^{-2x} \\ &= \frac{\rho_0}{fN}\frac{f(f-1)}{2}\left[\left(\frac{3}{4\pi}\right)^{3/2}\frac{\lambda_{\mathrm{b}}}{R^3}\right]\end{aligned} \tag{54}$$

In the second line, we have inserted $p_0 = \frac{\rho_0 \lambda_\mathrm{b}}{N}$, which is valid in the dilute regime. The density of a single star is $\frac{\rho_0}{fN}$, the combinatorial factor $\frac{f(f-1)}{2}$ is the total number of arm-to-arm pairs per star, and the remaining term in the bracket is the probability of linking two arm ends from Gaussian chain statistics.

The second contribution to the variation in bond density, due to excluded volume interaction, is negligible compared to the self-loop contribution. This is seen by noting that the Gaussian free energy contribution that contains the excluded volume interaction can be expanded up to linear order in the dilute limit as

$$\Pi_{\mathrm{G,v}} = -\frac{1}{2}\,\rho_0 u_0 N \int \frac{\mathrm{d}\mathbf{k}}{(2\pi)^3}\,\hat{G} \tag{55}$$

which is always of the linear order in ρ_0. Further substitution into eq. (32) leads to

$$\begin{aligned}\delta\rho_{\mathrm{b,v}} &= -\frac{1}{2}\rho_0 u_0 N \frac{p_0(1-p_0)}{1+p_0} \int \frac{\mathrm{d}\mathbf{k}}{(2\pi)^3}\,\frac{\partial \hat{G}}{\partial p_0} \\ &= -\frac{\lambda_\mathrm{b} u_0}{2}\rho_0^2 \int \frac{\mathrm{d}\mathbf{k}}{(2\pi)^3}\,\frac{\partial \hat{G}}{\partial p_0}\end{aligned} \tag{56}$$

In the dilute limit, p_0 and ρ_0 are in proportion, $p_0 = \frac{\rho_0 \lambda_\mathrm{b}}{N}$, as demanded by the LMA, eq. (19). So the correction $\delta\rho_{\mathrm{b,v}}$ is of order ρ_0^2, which can be neglected when compared to $\delta\rho_{\mathrm{b,l}}$. Therefore, it is clear that, in the dilute regime, the extra bonds contribute only to the formation of intra-star loops.

5.5 Dense melt

As a final illustration of the Gaussian fluctuation analysis, we consider the limit of a molten, solvent free system. The melt limit with finite ρ_0 is obtained by taking u_0 very large to suppress density variations. When this is done, the parameter u_0 is viewed as a compressional modulus of the melt. Its value can be determined from the density of state for ρ_0 when needed. However, in practice, it is more convenient to suppress u_0 and focus on the

density ρ_0. The fluctuation effects captured by the Gaussian analysis are caused by variation in compositions and spatial arrangement of clusters, while maintaining a spatially uniform density. Keeping the leading term of the integrand for $\Pi_{\rm G}$, while dropping an inconsequential factor $\ln(\rho_0 u_0 N)$ in the integrand, we have

$$\Pi_{\rm G} = -\frac{1}{2}\int \frac{{\rm d}\mathbf{k}}{(2\pi)^3} \ln\left(\hat{\Delta}\hat{G}\right) = -\frac{1}{2}\int \frac{{\rm d}\mathbf{k}}{(2\pi)^3} \ln\left(\hat{g}\hat{\Delta} + \hat{h}^2\hat{\Lambda}\right) \tag{57}$$

Here $\hat{\Lambda} \equiv f{-}1 + p_0 + 2p_0(f{-}1){\rm e}^{-x}$. While every term in the integrand depends on $x = k^2R_{\rm g}^2$, only $\hat{\Delta}$ and $\hat{\Lambda}$ depend on p_0. The dependence on density ρ_0 is implicit, via the equation of state for p_0, eq. (19).

Since the loop density has an identical form as for phantom stars at the Gaussian level, we focus on the variation in bond density. Substituting eq. (57) in eq. (32) gives

$$\delta\rho_{\rm b} = \frac{p_0(1-p_0)}{2(1+p_0)}\int \frac{{\rm d}\mathbf{k}}{(2\pi)^3} H(x), \tag{58}$$

$$H(x) \equiv \frac{(f{-}1){\rm e}^{-2x}\hat{g} - [1 + 2(f{-}1){\rm e}^{-x}]\hat{h}^2}{\hat{g}\hat{\Delta} + \hat{h}^2\hat{\Lambda}} \tag{59}$$

The integrand approaches $-(1{+}p_0)^{-1}$ as $k \to 0$, causing no difficulty in numerical evaluation. However, eq. (58) is divergent in the high k or ultraviolet (UV) regime. The exponential terms ${\rm e}^{-2x}$ and ${\rm e}^{-x}$ are negligible in this regime, so that $\hat{\Delta} \to 1$, $\hat{\Lambda} \to (f{-}1) + p_0$, $\hat{g} \to \hat{g}_\infty = \frac{2}{x} - \frac{2}{x^2}$, and $\hat{h} \to \hat{h}_\infty = \frac{1}{x}$. The integrand therefore behaves asymptotically as

$$-\frac{\hat{h}_\infty^2}{\hat{g}_\infty + [(f{-}1) + p_0]\hat{h}_\infty^2} = -\frac{1}{2x} + \mathcal{O}(x^{-2}) \tag{60}$$

Except the leading term $-1/(2x)$, all the higher order terms are UV convergent. Based on our analysis of the RPA structure factor, the term $\hat{h}_\infty^2$ is due to the bonding between arms on two neighboring stars. The term $\hat{g}_\infty$ captures the self-correlation of a single arm. The term $[(f{-}1) + p_0]\hat{h}_\infty^2$ gives the correlation between a randomly selected arm and the $(f{-}1)$ arms belonging to the same star, as well as one bonded arm from a neighboring star. The

diverging factor $-1/(2x)$ originates from the leading term in $-\hat{h}^2_\infty/\hat{g}_\infty$.

The physical reason for the divergence in high-k regime is the break-down of random walk statistics at small scale. To proceed, we observe that setting $N \to \infty$ gives the same integrand as the divergent contribution, $-1/(2x)$. Therefore, the integral can be renormalized by choosing a melt of stars with $N \to \infty$ as reference. Since the mean-field theory is expected to be exact in this limit, the value of $\delta\rho_{\mathrm{b},\infty}$ obtained using the structure factor with the correct liquid-state packing will *vanish*. Choosing this $N \to \infty$ system as reference amounts to subtracting the factor $-1/(2x)$ from the integrand. We therefore have the following renormalized form of $\delta\rho^*_\mathrm{b} = \delta\rho_\mathrm{b} - \delta\rho_{\mathrm{b},\infty}$

$$\delta\rho^*_\mathrm{b} = \frac{p_0(1-p_0)}{2(1+p_0)} \int \frac{\mathrm{d}\mathbf{k}}{(2\pi)^3} \left(H(x) + \frac{1}{2x} \right), \tag{61}$$

This scheme effectively renormalizes the value of the bonding activity λ_b, which now should be understood as the value attained in a melt with $N = \infty$. In practice, this bonding activity can be calibrated by (1) first measuring the conversion p_0 for star polymers with large N values, so that the fluctuation correction is small, (2) then using eq. (19) to calculate λ_b from p_0 and the known value of ρ_0. Such renormalization is necessary only because we adopted the random walk as a coarse-grained description to the structural correlation of real polymers, and the apparent divergence should not be present for a structural model with proper liquid-state details.

Equations (61) and (48) can be combined with eq. (31) to obtain the change in polymer number density. Before presenting the numerical results, the scaling with the system parameters is analyzed. First, the loop and bond densities can be normalized by the arm number density ρ_0/N. Second, since $R_\mathrm{g} = 6^{-1/2}R$ is the only length scale in the $\mathbf{k}$ integral of eq. (58), the wavenumber can be scaled by setting $q \equiv kR_\mathrm{g}$. By completing the integration over the azimuthal and polar angles, this brings out a factor $\frac{6^{3/2}}{2\pi^2 R^3}$, leaving only the radial

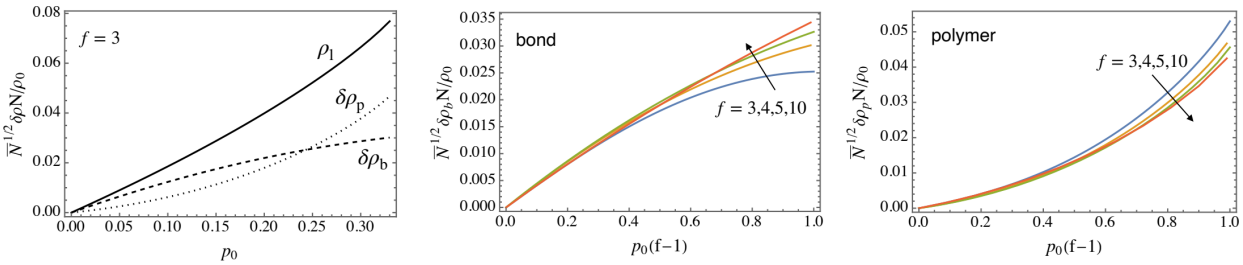

Figure 7: Variation of bond, loop, and polymer densities under melt conditions ($f = 3$). The dependence of $\delta\rho_{\rm b}$ and $\delta\rho_{\rm p}$ on $\bar{N}^{-1/2}$ and the convergence with increasing f are governed mainly by the product $p_0(f-1)$.

integration over $0 < q < \infty$. Therefore, we have ($z \equiv p_0(f-1)$)

$$\frac{N}{\rho_0}\rho_{\rm l} = \frac{N}{\rho_0 R^3}\left[\left(\frac{3}{4\pi}\right)^{3/2}\frac{{\rm Li}_{5/2}(z)}{2}\right] \tag{62}$$

$$\frac{N}{\rho_0}\delta\rho_{\rm b} = \frac{N}{\rho_0 R^3}\left[\frac{p_0(1-p_0)}{1+p_0}\frac{6^{3/2}}{4\pi^2}\int_0^\infty {\rm d}q\, q^2\left(H(x)+\frac{1}{2x}\right)\right] \tag{63}$$

where $H(x)$ is defined in eq. (59) and $x = q^2$. The asterisk on the renormalized bond density has been dropped for simplicity of notation going forward. The factor outside the bracket is recognized as $\bar{N}^{-1/2}$, with $\bar{N} \equiv (\rho_0 R^3/N)^2$ being the invariant degree of polymerization.[50] The parameter $\bar{N}$ counts the degree of inter-chain overlap, and therefore controls the strength of the fluctuation contributions. The behaviors of both $\rho_{\rm l}$ and $\delta\rho_{\rm b}$ are fully analogous to the scaling for fluctuation effects in block polymers[51,52] and several other examples surveyed.[50] Therefore, we are led to the following scaling

$$\rho_{\rm l} \sim \delta\rho_{\rm b} \sim \delta\rho_{\rm p} \sim \frac{1}{\bar{N}^{1/2}}\frac{\rho_0}{N} \tag{64}$$

for the Gaussian fluctuation theory. Such dependence naturally reflects the fact that the ability of an arm to bond with another one in the neighborhood depends on the degree of inter-chain overlap. The convergence towards the mean-field behavior is controlled by $\bar{N}^{-1/2}$.

Numerical results for the normalized $\rho_{\rm l}$, $\delta\rho_{\rm b}$ and $\delta\rho_{\rm p}$ are shown in Fig. 7. We focus on $\delta\rho_{\rm b}$ and $\delta\rho_{\rm p}$ because $\rho_{\rm l}$ is the same as the case of phantom stars. The variation $\delta\rho_{\rm b}$ includes

contributions from loop formation and excluded volume interaction, the latter resulting from the constraint of constant melt density. The number of extra bonds associated with loop formation is the same as for phantom stars, which is comparable to $\rho_{\rm l}$ and may exceeds $\rho_{\rm l}$ for large f values (Fig. 6).

Our result in Fig. 7a shows that $\delta\rho_{\rm b}$ is always less than $\rho_{\rm l}$, causing $\delta\rho_{\rm p}$ to increase monotonically. This implies that the excluded volume has reduced bond formation resulting in more polymers. Such reduction is anticipated for finite N values, and can be attributed to the effects of a correlation hole. For finite N values, the fraction of non-reacting middle segments in the arms increases, which dilutes the concentration of reacting end groups. As a result, the number of inter-molecular bonds is suppressed, compared to formation of intra-molecular bonds resulting in loops. The net result is the increment of $\delta\rho_{\rm p}$, the delayed growth of large clusters, and a delayed gel point.

The competition of $\rho_{\rm l}$ and $\delta\rho_{\rm b}$ depends only weakly on the value of f, when the conversion is represented as $z = p_0(f-1)$, which measures the distance to the mean-field gel point (Fig. 7). The normalized results converge for large f, which suggests a convenient way to analyze data from systems with variable $\bar{N}$ and f values.

5. Conclusions

We have constructed a coherent states model of f-arm star polymers with reversibly reacting ends in solution or molten conditions and applied approximate analytical techniques to interrogate phase behavior and gelation. At the mean-field level, this model reproduces the Flory-Stockmayer threshold for gelation, includes only tree-like clusters and no loops, and the mean-field condition is found to coincide with the equation of the gel fraction. In this particular bonding scheme, the system can phase separate into a polymer-lean supernatant sol, coexisting with a polymer rich gel, and spinodal decomposition can only occur after crossing the gelation threshold. This suggests strong kinetic limitations and path dependence

in experimental investigations.

In analyzing fluctuation corrections to the mean-field analysis, we discovered that only two independent densities, for loops and bonds, are needed. An expression for the bond density can be derived from a thermodynamic derivative involving the bonding activity (or equilibrium constant) for the reversible reaction. To obtain the loop number density, a loop density operator was developed by analyzing the spatial translation of crosslinked clusters. We argue that the loop density operator counts loops by summing up the compression factors of all arms belonging to a cluster.

At the Gaussian level of fluctuations, we analyzed the variation of loop number and bond number due to fluctuations in crosslinking pattern and excluded volume interactions. In the dilute limit, we show that the bonds are formed to create intra-star loops. In the limit of a dense melt, the Gaussian theory is UV divergent, but can be renormalized by choosing a fictitious melt of stars with infinitely long arms as a reference. The renormalized theory shows that the fluctuation correction to densities of bonds, loops, and clusters, when normalized by the star density ρ_0/N, all scale as $\bar{N}^{-1/2}$, where $\bar{N}$ is the invariant degree of polymerization, which places a bound on the rate of convergence towards the mean-field theory. The fluctuation correction for all three densities are positive. The fluctuation in loop number has to be positive since it is strictly zero in the mean-field approximation. The rate of increment of bond density is lower than that of the loop number density because the finite fraction of middle star segments depletes free ends slightly; a consequence of the correlation hole. The difference of the two gives the net change in the number density of polymers or clusters. The variation of these densities, when plotted against the product $p_0(f-1)$, with p_0 the fractional conversion in the mean-field reference, saturate when the number of arms f is high. The product $p_0(f-1)$ equals $1+\epsilon$, where ϵ is the degree of gelation parameter suggested by Flory.

One intriguing result of our work is that the excluded volume interaction does not influence the counting of loops at the Gaussian level. This allows one to split the fluctuation

contribution to the osmotic pressure according to $\Pi_G = \rho_l + \Pi_{G,v}$, with ρ_l the loop density and where the excluded volume interaction term $\Pi_{G,v}$ only alters the bond number density. A more complete diagrammatic analysis shows that at least cubic order couplings are required in the theory for excluded volume effects to be manifest in the loop density. The effects of such higher-order couplings will be examined in the future. Other important questions, such as the impact of loop density on the shift of the gel point and network elasticity, will be studied after an adequate treatment of excluded volume effects is in hand.

The current work provide the foundation for systematically incorporating fluctuation effects. Several future developments based on this can be envisioned. First, we have briefly discussed the possibility that the formation of loops may exhaust all reacting arms and suppress gelation in the dilute regime (Sec. 5.3). This clearly will affect the competition between gelation and phase separation, and can be examined after the fluctuation effects on phase separation is treated. Second, formation of loops delays the gel point. Our explicit expressions for the variations in bond number density and loop number density can be combined with the Stockmayer analysis[36,42] of heterogeneous reacting species to find out how the invariant arm length $\bar{N}$ influences the shift in the gel point. Third, extending our analysis to the post-gel regime and analyzing the network elasticity will be of great practical value. In this regime, the saddle point condition has two solutions, one related to the percolating gel component and another related to the finite clusters (Sec. 3.2). It is possible to relate the value of the CST field $\phi^*(0)$ to the exiting probability $P(F_A^{out})$ introduced by Macosko-Miller in their analysis of network polymers.[5,6] A useful extension would be to combine our Gaussian fluctuation theory with the Macosko-Miller framework, to probe the post gel properties.

Acknowledgement

This work was supported by the CMMT Program of the National Science foundation, grant

number DMR-2104255. Acknowledgement is made to the Donors of the American Chemical Society Petroleum Research Fund for partial support of this research.

Supporting Information Available

Order parameter for gelation and critical point for phase separation (S1), connection between loop operator and compression factor (S2), algebraic derivation of the Gaussian free energy (S3), and diagrammatic expansion of the Gaussian free energy that reveals the crosslinking patterns included (S4).

References

(1) Cordier, P.; Tournilhac, F.; Soulié-Ziakovic, C.; Leibler, L. Self-healing and thermoreversible rubber from supramolecular assembly. *Nature* **2008**, *451*, 977–980.

(2) Harmon, T. S.; Holehouse, A. S.; Rosen, M. K.; Pappu, R. V. Intrinsically disordered linkers determine the interplay between phase separation and gelation in multivalent proteins. *eLife* **2017**, *6*, e30294, DOI: 10.7554/eLife.30294.

(3) Flory, P. J. Molecular size distribution in three dimensional polymers I. Gelation. *J. Am. Chem. Soc.* **1941**, *63*, 3083–3090.

(4) Stockmayer, W. H. Theory of Molecular Size Distribution and Gel Formation in Branched-Chain Polymers. *The Journal of Chemical Physics* **1943**, *11*, 45–55, DOI: 10.1063/1.1723803.

(5) Miller, D. R.; Macosko, C. W. A new derivation of average molecular weights of nonlinear polymers. *Macromolecules* **1976**, *9*, 199.

(6) Macosko, C. W.; Miller, D. R. A new derivation of post gel properties of network polymers. *Macromolecules* **1976**, *9*, 206.

(7) Lubensky, T. C.; Isaacson, J. Field Theory for the Statistics of Branched Polymers, Gelation, and Vulcanization. *Phys. Rev. Lett.* **1978**, *41*, 829–832, DOI: 10.1103/PhysRevLett.41.829.

(8) Lubensky, T. C.; Isaacson, J. Statistics of lattice animals and dilute branched polymers. *Phys. Rev. A* **1979**, *20*, 2130–2146, DOI: 10.1103/PhysRevA.20.2130.

(9) Panyukov, S.; Rabin, Y. Statistical physics of polymer gels. *Physics Reports* **1996**, *269*, 1–131, DOI: https://doi.org/10.1016/0370-1573(95)00068-2.

(10) Goldbart, P.; Goldenfeld, N. Rigidity and ergodicity of randomly cross-linked macromolecules. *Phys. Rev. Lett.* **1987**, *58*, 2676.

(11) Goldbart, P.; Goldenfeld, N. Solid state of cross-linked macromolecules: basic concepts. *Macromolecules* **1989**, *22*, 948.

(12) Erukhimovich, I. Y. Statistical theory of the sol-gel transition in weak gels. *JETP* **1995**, *81*, 553.

(13) Ermoshkin, A. V.; Erukhimovich, I. Y. Toward a statistical theory of associating telechelics: Equilibrium molecular structural distribution and one-cluster static scattering. *J. Chem. Phys.* **1999**, *110*, 1781.

(14) Schwenke, K.; Lang, M.; Sommer, J.-U. On the Structure of Star–Polymer Networks. *Macromolecules* **2011**, *44*, 9464–9472, DOI: 10.1021/ma202022q.

(15) Lang, M.; Schwenke, K.; Sommer, J.-U. Short Cyclic Structures in Polymer Model Networks: A Test of Mean Field Approximation by Monte Carlo Simulations. *Macromolecules* **2012**, *45*, 4886–4895, DOI: 10.1021/ma300317z.

(16) Lang, M.; Muller, T. Analysis of the gel point of polymer model networks by computer simulations. *Macromolecules* **2020**, *53*, 498–512.

(17) Kumar, K. S.; Lang, M. Reversible Networks Made of Star Polymers: Mean-Field Treatment with Consideration of Finite Loops. *Macromolecules* **2023**, *56*, 7166–7183, DOI: 10.1021/acs.macromol.3c00796.

(18) Lang, M.; Scholz, R.; Müller, T. Impact of smallest loops and composition fluctuations on the structure of end-linked polymer model networks. *Polymer* **2025**, *330*, 128454, DOI: https://doi.org/10.1016/j.polymer.2025.128454.

(19) Mohan, A.; Elliot, R.; Fredrickson, G. H. Field-theoretic model of inhomogeneous supramolecular polymer networks and gels. *J. Chem. Phys.* **2010**, *133*, DOI: 10.1063/1.3497038/920802.

(20) Mester, Z.; Mohan, A.; Fredrickson, G. H. Macro- and microphase separation in multifunctional supramolecular polymer networks. *Macromolecules* **2011**, *44*, 9411–9423, DOI: 10.1021/MA201551C/ASSET/IMAGES/MA-2011-01551C_M075.GIF.

(21) Edwards, S. F.; Freed, K. F. Cross Linkage Problems of Polymers I. The Method of Second Quantization Applied to the Cross Linkage Problem of Polymers. *J. Phys. C: Solid State Phys.* **1970**, *3*, 739.

(22) Negele, J. W.; Orland, H. *Quantum Many-particle Systems (Advanced Books Classics)*; Addison-Wesley: New York, 1988.

(23) Edwards, S. F. The statistical mechanics of polymers with excluded volume. *Proc. Phys. Soc., London* **1965**, *85*, 613–624, DOI: 10.1088/0370-1328/85/4/301.

(24) Man, X.; Delaney, K. T.; Villet, M. C.; Orland, H.; Fredrickson, G. H. Coherent states formulation of polymer field theory. *J. Chem. Phys.* **2014**, *140*, 024905, DOI: 10.1063/1.4860978.

(25) Fredrickson, G. H.; Delaney, K. T. Coherent states field theory in supramolecular polymer physics. *J. Chem. Phys.* **2018**, *148*, 204904, DOI: 10.1063/1.5027582.

(26) Vigil, D. L.; Zhang, A.; Delaney, K. T.; Fredrickson, G. H. Phase Separation, Reaction Equilibrium, and Self-Assembly in Binary Telechelic Homopolymer Blends. *Macromolecules* **2023**, *56*, 9994–10005, DOI: 10.1021/ACS.MACROMOL.3C01653.

(27) Fredrickson, G. H.; Delaney, K. T. *Field-Theoretic Simulations in Soft Matter and Quantum Fluids*; Oxford University Press: Oxford, 2023; DOI: 10.1093/oso/9780192847485.001.0001.

(28) Balzer, C.; Fredrickson, G. H. Sequence and gelation in supramolecular polymers. *J. Chem. Phys.* **2024**, *161*, 54907, DOI: 10.1063/5.0218748.

(29) Semenov, A. N.; Rubinstein, M. Thermoreversible gelation in solutions of associating polymers. 1 statics. *Macromolecules* **1998**, *31*, 1373–1385.

(30) Erukhimovich, I. Y.; Ermoshkin, A. V. Phase diagrams classification of thermoreversibly associating systems with due regard for mesoscopic cyclization effects. *J. Chem. Phys.* **2002**, *116*, 368.

(31) Verduin, H.; Dhont, J. K. G. Phase diagram of a model adhesive hard-sphere dispersion. *J. Colloid and Interface Science* **1995**, *172*, 425.

(32) Miller, M. A.; Frenkel, D. Phase diagram of the adhesive hard sphere fluid. *J. Chem. Phys.* **2004**, *121*, 535.

(33) Lodge, T. P.; Hiemenz, P. C. *Polymer Chemistry*; CRC Press, 2020.

(34) Rubinstein, M.; Colby, R. H. *Polymer Physics*; Oxford University Press, 2003.

(35) Flory, P. J. *Principles of Polymer Chemistry*; Cornell University Press, 1954.

(36) Stockmayer, W. H. Theory of molecular size distribution and gel formation in branched polymers II. general cross linking. *J. Chem. Phys.* **1944**, *12*, 125–131.

(37) Amit, D. J. *Field Theory, The Renormalization Group and Critical Phenomena*, 2nd ed.; WORLD SCIENTIFIC, 1993; DOI: 10.1142/0064.

(38) Strauss, W. A. *Partial Differential Equations: An Introduction*; John Wiley & Sons, Inc., 1992.

(39) Stauffer, D.; Aharony, A. *Introduction to Percolation Theory*; Taylor & Francis, 1994.

(40) Read, D. J. Mean Field Theory for Phase Separation during Polycondensation Reactions and Calculation of Structure Factors for Copolymers of Arbitrary Architecture. *Macromolecules* **1998**, *31*, 899.

(41) Hammouda, B. Small-Angle Scattering from Branched Polymers. *Macrom. Theory Simul.* **2012**, *21*, 372.

(42) Jacobson, H.; Stockmayer, W. H. Intramolecular reaction in polycondensations. I. the theory of linear systems. *J. Chem. Phys.* **1950**, *18*, 1600.

(43) Hoeve, C. A. J. Molecular weight distribution of thermally polymerized triglyceride oils. II. Effect of intramolecular reaction. *J. Polym. Sci.* **1956**, *21*, 11.

(44) Leung, Y.-K.; Eichinger, B. E. Computer simulation of end-linked elastomers. I. Trifunctional networks cured in the bulk. *J. Chem. Phys.* **1984**, *80*, 3877.

(45) Lang, M.; Göritz, D.; Kreitmeier, S. Intramolecular reactions in randomly end-linked polymer networks and linear (co)polymerizations. *Macromolecules* **2005**, *38*, 2515.

(46) Wang, R.; Alexander-Katz, A.; Johnson, J. A.; Olsen, B. D. Universal cyclic topology in polymer networks. *Phys. Rev. Lett.* **2016**, *116*, 188302.

(47) Zhong, M.; Wang, R.; Kawamoto, K.; Olsen, B. D.; Johnson, J. A. Quantifying the impact of moleculardefects on polymer network elasticity. *Science* **2016**, *353*, 1264–1268.

(48) Ercolani, G.; Mandolini, L.; Mencarelli, P.; Roelens, S. Macrocyclization under Thermodynamic Control. A Theoretical Study and Its Application to the Equilibrium Cyclooligomerization of β-Propiolactone. *Macromolecules* **1993**, *115*, 3901.

(49) Suematsu, K. Recent Progress in Gel Theory: Ring, Excluded Volume, and Dimension. *Adv. Polym. Sci.* **2002**, *156*, 137.

(50) Qin, J. Similarity of polymer packing in melts in dicated by $\bar{N}$. *Macromolecules* **2024**, *57*, 1885.

(51) Fredrickson, G. H.; Helfand, E. Fluctuation effects in the theory of microphase separation in block copolymers. *J. Chem. Phys.* **1987**, *87*, 697.

(52) Bates, F. S.; Rosedale, J. H.; Fredrickson, G. H.; Glinka, C. J. Fluctuation-induced first-order transition of an isotropic system to a periodic state. *Phys. Rev. Lett.* **1988**, *61*, 2229.